



1 **Segregation in the Atmospheric Boundary Layer:**
2 **The Case of *OH* - Isoprene**

3
4
5 Ralph Dlugi^{1,2,3}, Martina Berger^{1,2,3}, Chinmay Mallik², Anywhere Tsokankunku^{2,3},
6 Michael Zelger^{1,2,3}, Otávio C. Acevedo⁴, Efstratios Bourtsoukidis², Andreas
7 Hofzumahaus⁵, Jürgen Kesselmeier³, Gerhard Kramm⁶, Daniel Marno², Monica
8 Martinez², Anke C. Nölscher², Huug Ouwersloot², Eva Y. Pfannerstill², Franz Rohrer⁵,
9 Sebastian Tauer², Jonathan Williams², Ana-Maria Yáñez-Serrano³, Meinrat O.
10 Andreae^{3,7}, Hartwig Harder² and Matthias Sörgel^{2,3}

11
12
13 ¹Arbeitsgruppe Atmosphärische Prozesse (AGAP), Munich, Germany

14 ²Atmospheric Chemistry Department, Max Planck Institute for Chemistry, P.O. Box
15 3060, 55020 Mainz, Germany

16 ³Biogeochemistry Department, Max Planck Institute for Chemistry, Mainz, Germany

17 ⁴Universidade Federal Santa Maria, Dept. Fisica, 97119900 Santa Maria, RS, Brazil

18 ⁵Institut für Energie- und Klimaforschung: Troposphäre, Forschungszentrum Jülich,
19 Germany

20 ⁶Engineering Meteorology Consulting, Fairbanks, AK, USA

21 ⁷Scripps Institution of Oceanography, University of California San Diego, California,
22 USA

23
24
25 *Correspondence to:* R. Dlugi (rdlugi@gmx.de) and M.Sörgel (m.soergel@mpic.de)

26
27
28 **Abstract**

29
30
31 In the atmospheric boundary layer (ABL), incomplete mixing (i.e., segregation) results in
32 reduced chemical reaction rates compared to those expected from mean values and rate
33 constants derived under well mixed conditions. Recently, segregation has been suggested
34 as a potential cause of discrepancies between modelled and measured OH radical
35 concentrations, especially under high isoprene conditions. Therefore, the influence of
36 segregation on the reaction of OH radicals with isoprene has been investigated by modelling
37 studies and one ground-based and one aircraft campaign.

38
39 In this study, we measured isoprene and OH radicals with high time resolution in order to
40 directly calculate the influence of segregation in a low-NO_x and high-isoprene environment in
41 the central Amazon basin. The calculated intensities of segregation (I_s) at the Amazon Tall
42 Tower Observatory (ATTO) above canopy top are in the range of values determined at a
43 temperate deciduous forest (ECHO-campaign) in a high-NO_x low-isoprene environment, but
44 stay below 10 %. To establish a more general idea about the causes of segregation and their
45 potential limits, further analysis was based on the budget equations of isoprene mixing ratios,



46 the variance of mixing ratios, and the balance of the intensity of segregation itself.
47 Furthermore, it was investigated if a relation of I_s to the turbulent isoprene surface flux can
48 be established theoretically and empirically, as proposed previously. A direct relation is not
49 given and the amount of variance in I_s explained by the isoprene flux will be higher the less
50 the influence from other processes (e.g., vertical advection) is and will therefore be greater
51 near the surface. Although ground based values of I_s from ATTO and ECHO are in the same
52 range, we could identify different dominating processes driving I_s . For ECHO the normalized
53 variance of isoprene had the largest contribution, whereas for ATTO the different transport
54 terms expressed as a residual were dominating. To get a more general picture of I_s and its
55 potential limits in the ABL, we also compared these ground based measurements to ABL
56 modelling studies and results from an aircraft campaign. The ground based measurements
57 show the lowest values of the degree of inhomogenous mixing (< 20 %, mostly below 10 %).
58 These values increase if the contribution of lower frequencies is added. Values integrated
59 over the whole boundary layer (modelling studies) are in the range from 10 % to 30 % and
60 aircraft measurements integrating over different landscapes are amongst the reported. This
61 presents evidence that larger scale heterogeneities in land surface properties contribute
62 substantially to I_s .

63

64

65 1. Introduction

66

67 Reaction rates of atmospheric trace gases can deviate from the ones derived in laboratory
68 experiments because the reactants might not be well mixed (i.e., they are segregated).
69 Mixing in the atmospheric boundary layer (ABL) is provided by shear-generated turbulence
70 or by convection. Therefore, mixing of the reactants will depend on the turbulence properties
71 of the airflow. To achieve well-mixed conditions, the mixing has to overcome the influences of
72 heterogeneous source and sink distributions of the reactants due to fluxes into and out of the
73 reaction volume and due to chemical reactions inside the volume. Thus, chemistry and
74 turbulent properties need to be considered together (e.g., Seinfeld and Pandis, 1997;
75 Finlayson-Pitts and Pitts Jr., 1986; Lamb and Seinfeld, 1973; Donaldson, 1975). Most
76 models consider chemical reactions of first, second, and third order in a way that mean
77 mixing ratios \bar{c}_i and their products (e.g., $\bar{c}_i \times \bar{c}_j$ for a second-order reaction) together with the
78 rate constant k_{ij} appear in the rate equations, as determined from laboratory experiments
79 (e.g., Finlayson-Pitts and Pitts Jr., 1986). In the atmosphere, conditions often occur where
80 the reactants are not well mixed with significant fluctuations, c'_i and c'_j , compared to their
81 mean values, \bar{c}_i and \bar{c}_j . For those cases, also additional terms like variances and
82 covariances, $\overline{c'_i c'_j}$, have to be considered (e.g., O'Brien, 1971; Lamb and Seinfeld, 1973; Shu,



83 1976; McRae et al., 1982; Donaldson and Hilst, 1972; Donaldson, 1975; Lamb and Shu,
84 1978). Here, c'_i and c'_j denote temporal fluctuations around the mean mixing ratios, \bar{c}_i and \bar{c}_j ,
85 of compounds i and j , respectively. If for a second-order reaction the product of the mean
86 mixing ratios fulfills the relation $\bar{c}_i \times \bar{c}_j \gg \overline{c'_i c'_j}$, the influence of turbulent fluctuating terms in
87 the reaction rate equation $k_{ij} (\bar{c}_i \times \bar{c}_j + \overline{c'_i c'_j})$ can be neglected for the prediction of either
88 mean value, \bar{c}_i or \bar{c}_j (e.g., Danckwerts, 1952; Shu, 1976).

89

90 If this inequality is not valid, the balances of higher order moments (e.g., variances,
91 covariances, triple correlations) have to be calculated either by the model or by analysis of
92 experimental data. The quotient of the covariance term and the product of the means is
93 commonly called the intensity of segregation, $I_s = (\overline{c'_i c'_j} / \bar{c}_i \times \bar{c}_j)$ (e.g., Danckwerts, 1952;
94 Damköhler, 1957) and is applied to describe the degree of inhomogeneous mixing for
95 second order chemical reactions. For this Reynolds-type ensemble averaging of properties of
96 a fluid, the influence of fluctuations on chemical reactions is described by additional
97 differential equations to determine the higher-order moments (e.g., Donaldson and Hilst,
98 1972; Donaldson, 1973, 1975; Shu, 1976). Another way to approach this problem is to find
99 the exact properties of the probability density functions of turbulent quantities for each
100 reactant (e.g., O'Brien, 1971; Bencula and Seinfeld, 1976; Lamb and Shu, 1978).

101

102 The balance equation approach was also applied for the analysis of field measurements of
103 the $O_3 - NO - NO_2$ system (e.g., Lenschow, 1982; Vilà - Guerau de Arellano et al., 1993;
104 Kramm and Meixner, 2000) and to study segregation of the reaction of isoprene (*ISO*) with
105 the hydroxyl radical (*OH*) (Dlugi et al., 2010, 2014). This concept not only considers the
106 determination of first- and second- order moments (mean values, covariances and variances)
107 but at least requires the additional knowledge of the third moments – e.g., the skewness, Sk
108 (Stull, 1988; Sorbjan, 1989; Shu, 1976) - to quantify influences of so-called *coherent*
109 *structures* (e.g., Katul et al, 1997, 2006; Raupach et al., 1996; Wahaft, 2000) on
110 segregation (e.g., Dlugi et al., 2014).

111

112 Modelling studies on segregation for these chemical systems were mainly performed for
113 more complex atmospheric mixtures (e.g., Schumann, 1989; Verver et al., 1997; Vinuesa
114 and Vilà-Guerau de Arellano, 2005; Krol et al, 2000; Ouwersloot et al., 2011; Ebel et al.,
115 2007; Patton et al., 2001; Kim et al., 2016; Li et al., 2016; Gerken et al., 2016) than could be
116 considered by the analysis of field data (Dlugi et al., 2010, 2014; Kaser et al., 2015; Kramm
117 and Meixner, 2000). Recently, the influences of shallow cumulus on transport, mixing and
118 chemical reactions in the ABL were modelled for the reaction *isoprene* + *OH* (e.g., Vilà-



119 Guerau de Arellano et al., 2005; Ouwersloot et al., 2013; Kim et al., 2016; Li et al., 2016).
120 The dynamics and mixing by shallow cumulus clouds are shown to enhance I_s also near the
121 surface at least in qualitative agreement with the scarce experimental findings (Dlugi et al.,
122 2014).

123

124 For a characterization of mixing and reaction conditions in atmospheric flows, the Damköhler
125 number, Da_c , the quotient (τ_t/τ_c) between the characteristic timescales of turbulent or
126 convective mixing processes, τ_t , and the specific chemical reaction, τ_c , of a compound (e.g.,
127 *ISO* or *OH*), is chosen (e.g., Vilá Guereau de Arellano and Lelieveld, 1998). This
128 dimensionless number allows a classification of I_s as a function of nearly inert ($Da_c \ll 1$),
129 slow ($0.05 \leq Da_c \leq 0.5$), fast ($0.5 \leq Da_c \leq 5$), and very fast ($Da_c > 5$) bimolecular reactions
130 with respect to one of the two reactants. Damköhler numbers can be formulated in different
131 ways in space and time, depending on the formulation of the turbulence scales (e.g.,
132 Donaldson and Hilst, 1972; Molemaker et al., 1998; Koeltzsch, 1998). Therefore, the actual
133 numerical values of Da_c in various works found in the literature may differ systematically
134 (e.g., Schumann, 1989; Sykes et al., 1994; Verver et al., 1997, 2000; Li et al., 2016).
135 Nevertheless, the ranking of reactions being most influenced by inhomogeneous mixing is
136 consistent within each choice of scales for the calculation of Da_c .

137

138 Some authors applied an additional scaling which uses the turbulent flux of a species
139 (e.g., $\overline{w'c'_i}$) at the surface to find a description for the reaction and inhomogeneous mixing
140 (e.g., Schumann, 1989; Verver et al., 2000) and added a second Damköhler number, Da_f , to
141 describe the influence of the surface flux on this ranking concept. This approach requires that
142 for a specific reaction (e.g., *ISO* + *OH*) the segregation intensity, I_s , shows a clear functional
143 dependence on the corresponding turbulent flux. We will therefore discuss this concept
144 together with the theoretical framework applied to the analysis of the field data in Section 3.
145 In Sections 3.4 and 4.1 we search for theoretical and empirical relations between the
146 turbulent flux of isoprene and the related segregation intensity to test this hypothesis,
147 because some studies suggest that spatially inhomogeneous distributions of emission fluxes
148 significantly influence – in a direct relation – the segregation intensity (e.g., Krol et al., 2000;
149 Pugh et al., 2011; Ouwersloot et al., 2011). The results from the aircraft measurements
150 presented by Kaser et al. (2015) are interpreted in this way as well. They even suggest a
151 “feedback loop – the higher the isoprene flux the larger the I_s ”. The analysis of ECHO 2003
152 by Dlugi et al. (2014) showed that such an influence of spatially variable isoprene fluxes can
153 be detected also in the results from measurements near canopy top, but needs a more
154 specific interpretation (section 3.4).

155



156 One of the chemical reactions that has been studied experimentally is that of isoprene with
157 *OH* radicals. Isoprene is an important biogenic compound with a global annual emission of
158 535 Tg/a to 595 Tg/a (Sindelarova et al., 2014; Guenther et al., 2012). If also the
159 dependence on soil moisture stress is considered an annual emission of about 374 –
160 449 T is estimated (Müller et al., 2008). Isoprene is emitted by various plants (Kesselmeier,
161 2001; Kesselmeier and Staudt, 1999; Günther et al., 1995). The emission source strength
162 and related fluxes into the atmosphere are mainly controlled by plant physiological factors,
163 absorbed radiation and leaf temperatures (e.g., Kesselmeier, 2001; Guenther et al., 2006;
164 Ciccioli et al., 1997; Doughty, Goulden, 2008). After emission, isoprene is mixed by
165 turbulence and convection in a cloud topped ABL (e.g., Heus and Jonker, 2008; Ramos da
166 Silva et al., 2011; Ouwersloot et al., 2013), while being transported with the mean wind field.
167 Isoprene reacts with *OH* (e.g., Finlayson-Pitts and Pitts Jr., 1986), the so called *detergent of*
168 *the atmosphere*, which is formed by photochemical reactions and recycled in *radical chain*
169 *reactions* (e.g., Finlayson – Pitts and Pitts, 1986; Rohrer et al., 2014). It is a fast reacting
170 compound with $\tau_c < 1s$. Therefore, the hydroxyl radical (*OH*) is only locally determined by
171 chemical sources and sinks which are influenced by the solar actinic flux, ozone (O_3), water
172 vapor and additional reactants like HO_2 , NO_2 , NO , CO , CH_4 and various volatile organic
173 compounds (VOCs). We may consider this chemical system in the way that isoprene (with
174 $\tau_c > 300s$) is transported through this locally variable field of *OH*. Furthermore, the variability
175 of the isoprene source strength in time and space (e.g., Ciccioli et al., 1997) – which may be
176 described by the turbulent surface flux of isoprene $\overline{w'c'_i}$ - as well as of chemical sources and
177 sinks of *OH* can contribute to the development of non-homogeneously mixed conditions
178 with $I_s < 0$ (e.g., Krol et al., 2000; Ouwersloot et al., 2011; Dlugi et al., 2014). For the further
179 analysis, the Damköhler number, Da_c , is used as a scale for the chemical reactant isoprene
180 (*ISO*) with respect to the active species (*OH*).

181

182 This chemical system and its behavior in the ABL were analyzed by model studies for
183 isoprene in a complex chemical mixture (Verver et al., 2000; van Stratum et al., 2012; Kim et
184 al., 2016; Li et al., 2016). Patton et al. (2001) performed a Large Eddy Simulation (LES)
185 study for isoprene in a mixture with CO to assess the influences of emission, mixing and
186 reaction on the intensity of segregation, I_s , in the roughness sublayer (Raupach et al., 1996)
187 within and directly above an idealized deciduous forest. All analyses found $I_s < 0$ near the
188 bottom – e.g., canopy top - of their models, which is caused by an anti-correlation between
189 the reacting compounds.

190

191 Ouwersloot et al. (2011) also applied LES to model mechanically and thermally generated
192 turbulence above a differentially heated land surface representing alternating forest and



193 savanna areas. This inhomogeneity of land surface properties (and of canopy surface
194 temperatures and surface sensible heat fluxes, H_s) is related to variations in buoyant
195 production as well as inhomogeneous source distributions for isoprene, both of which have
196 an impact on the variability of the isoprene flux and the mixing ratio (e.g., the variance) and,
197 therefore, on I_s for the isoprene – OH reaction. Comparable to the study by Patton et al.
198 (2001), the modelled chemical reactions are for low NO_x conditions as found for example in
199 the Amazonian region (e.g., Rohrer et al., 2014) - where one major sink for OH is isoprene
200 (e.g., Andreae et al., 2015; Karl et al., 2007; Nölscher et al., 2015; Yáñez- Serrano et al,
201 2015).

202

203 In their LES simulation, Kim et al. (2016) found that I_s is a function of the NO_x mixing ratio.
204 They point out that values with $I_s < -0.1$ both for $NO_x < 0.2$ ppb and $NO_x > 1$ ppb are
205 reached in a cloud layer. Positive values of I_s are calculated in the cloud layer for $NO_x \approx$
206 0.5 ppb. In the mixed layer of the ABL Kim et al. (2016) found $I_s < -0.1$ only for $NO_x \geq 3$ ppb.
207 Their surface layer (SL) results are nearly independent from the NO_x mixing ratios with
208 $-0.05 \leq I_s \leq 0.0$ for a homogeneous isoprene flux. In contrast, near the surface Ouwersloot
209 et al. (2011) found significantly larger values for low NO_x - conditions, but in a region with
210 inhomogeneous distributions of the surface sensible heat flux H_s and the isoprene emission
211 flux $\overline{w'c'_i}$. In their Fig. 13 they show a case with $I_s = -0.195$ and $H_s \approx 0.15$ Kms^{-1} for an
212 inhomogeneous distribution of the isoprene emission flux. But most of their results for
213 homogeneous source distributions are in the range $I_s < -0.1$ and are at least qualitatively
214 comparable to the results of Kim et al. (2016). The experimental values determined above
215 canopy top during the ECHO 2003 field study with $NO_x > 1$ ppb are in the range $-0.16 < I_s \leq$
216 0 with the largest values determined for convective conditions in a cloud topped ABL (Dlugi
217 et al. 2010, 2014).

218

219 Pugh et al. (2011) applied results from the field study ECHO 2003 (Dlugi et al., 2010) to
220 estimate a potential influence of segregation for the reaction $ISO + OH$ on results of another
221 field study above tropical rain forest in Indonesia, although the level of NO_x - compounds
222 significantly differs from those at the deciduous forest of the ECHO site. For the Amazonian
223 region, Butler et al. (2008) estimated that values of $-0.6 \leq I_s \leq -0.3$ are needed to interpret
224 their chemical measurements with an aircraft in the upper ABL during the GABRIEL field
225 campaign. But, after an extended error analysis, these authors estimated an average value
226 of $I_s \approx -0.13$, about the largest value later on given by Dlugi et al. (2010, 2014) from direct
227 measurements near the surface or by Ouwersloot et al. (2011) in their model study.

228



229 Dlugi et al. (2010, 2014) analyzed highly time-resolved (≤ 0.2 Hz) data from measurements
230 of isoprene and OH during the ECHO 2003 field experiment above a deciduous forest
231 canopy in a polluted area (e.g., $NO_x > 1$ ppb). They could specify influences of
232 inhomogeneous source distribution, turbulence, and cloud-induced convective downward
233 and upward transport on I_s in the range $-0.16 < I_s \leq 0$ for the reaction between isoprene
234 and OH . In addition, they found for their experimental data that the time variation of the
235 covariance between isoprene (c_i) and $OH(c_j)$, $d(\overline{c'_i c'_j})/dt = S_{cov}$, was significantly smaller
236 than all other terms in the prognostic equation for $\overline{c'_i c'_j}$. This allowed them to derive a
237 diagnostic equation for I_s (based on the stationarity condition $S_{cov} = 0$) to separate influences
238 of the complex interactions of mixing processes as a residuum (RE_{is}) from measurable
239 quantities in the flow, like the normalized variance of isoprene, $nvar(ISO)$. Using this
240 concept, they were able to compare their experimental findings with model results given by
241 Ouwersloot et al. (2011) and Patton et al. (2001). They verified that $nvar(ISO)$ and RE_{is} both
242 can be related to the influence of coherent motion near canopy top in a way that these terms
243 correlate with the generalized correlation coefficient M_{21} for the turbulent transport of
244 $nvar(ISO)$ as formulated by Katul et al. (1997) and Cava et al. (2006) by the third-order
245 cumulant expansion method (CEM). I_s correlates not only with the (normalized) variance of
246 isoprene but also with the turbulent flux of variance, and, therefore also well with the quantity
247 $(nvar(ISO) - RE_{is})$ (Dlugi et al. 2014). In contrast, they found little to no correlation between
248 I_s and the corresponding correlation coefficient M_{12} for the turbulent transport of the isoprene
249 flux $\overline{w'c'_i}$ given by CEM. We refer to this result in Section 4.2.2.

250

251 Recently Kaser et al. (2015) published their results from the NOMADSS campaign on
252 segregation in the system isoprene + OH from airborne measurements in the ABL for a flight
253 level of about $z/z_i = 0.4$ (z = height above ground; z_i = ABL height). They determined a
254 significant spatial variability of I_s during two flights (RF13, RF17). In addition, they presented
255 LES model simulations in the range of $-0.35 < I_s \leq -0.06$ with a qualitative agreement with
256 their experimental results near $z/z_i \approx 0.4$ but significantly larger values up to about $I_s \approx -0.4$
257 near the canopy top level compared to results from the other studies. Furtheron, they also
258 suggest that a statistically significant relationship between the turbulent flux of isoprene $\overline{w'c'_i}$
259 and I_s exists. In addition, they stated that the covariance $\overline{c'_i c'_j}$ is directly proportional to I_s ,
260 which implies that the product of mean mixing ratios $\overline{c_i} \times \overline{c_j}$ is of minor influence.

261

262 In the following Section 2 we summarize the three field studies for which experimental data
263 on segregation for the reaction *isoprene* + OH are available. These studies are ECHO 2003,



264 ATTO 2015 (see Sections 2.2, 3. and 4.), and NOMADSS (Kaser et al., 2015). In our
265 discussion in Section 3 we present the theoretical frameworks, which serve as a rule on how
266 to perform atmospheric measurements of this kind and to analyze the data. As introduction
267 we give the definition of I_s and explain the different influences of the mean mixing ratios of
268 $ISO(\bar{c}_i)$ and $OH(\bar{c}_j)$, their related standard deviations (σ_i, σ_j) and variances ($\overline{c_i'^2}, \overline{c_j'^2}$), their
269 covariance ($\overline{c_i'c_j'}$) and the isoprene flux ($\overline{w'c_i'}$). For each of these quantities a prognostic
270 balance equation (also named budget equation in the literature) allows us to analyze the
271 impact of different processes on their behavior in time and space (e.g., Stull, 1988; Sorbjan,
272 1989; Seinfeld and Pandis, 1997). These processes are represented by the different terms of
273 the balance equations as described for the exchange and transport of momentum, heat, and
274 moisture for example by Monin and Obukhov (1954), Businger (1973), McBean and Miyake
275 (1972), Panofsky and Dutton (1994), Stull (1988), Sorbjan (1989) or Garrett (1992) and for
276 reacting compounds for example by Shu (1976), McRay et al. (1982), Lenschow (1982) or
277 Ebel et al. (2007). This kind of analysis is done by solving these equations numerically in a
278 model or by calculation of the different terms from direct measurements and order of
279 magnitude estimates based on literature values, as also done in our study.

280

281 First, we perform such calculations for the balance of the mean mixing ratio \bar{c}_i based on the
282 data from ECHO 2003 and ATTO 2015 (Section 3.2). Secondly, we discuss the balances of
283 the variances, as they can be directly related to the covariance, $\overline{c_i'c_j'}$, and to the segregation
284 intensity, I_s (Section 3.3). In the following Section 3.4 we focus on the balance of the
285 isoprene flux, $\overline{w'c_i'}$, to analyze if a direct relation to I_s can be established by a term of this
286 equation, as suggested, for example, by Kaser et al. (2015). Finally, the balance of the
287 segregation intensity, I_s , itself is evaluated based on measurements. In Section 4 we
288 compare results from earlier modelling studies and direct field measurements near canopy
289 top to each other and to the findings given by Kaser et al. (2015) from experiments in the
290 ABL. The results from experiments in the atmosphere and modelling studies are compared
291 also to obtain some empirical relation between the segregation intensity I_s and the
292 Damköhler number Da_c .

293

294

295

296

297 2. The Field Studies

298



299 **2.1. ECHO 2003**

300

301 The ECHO intensive field campaign was performed from 17 June to 6 August 2003 on the
302 grounds of the Reserch Center Jülich, Germany. Three towers were installed in a mixed
303 deciduous forest with the dominating tree species, beech, birch, oak and ash, and a mean
304 canopy height h_c of 30 m. The vertically integrated one-sided leaf area index in a radius of 50
305 m around the main tower varied between $LAI = 5.5$ and $LAI = 5.8$. The towers were aligned
306 parallel to the main wind direction (Schaub, 2007) with the main tower in the center. The
307 west tower was located 220 m from the main tower, and the east tower was located 120 m
308 away. This allowed the investigation of the influence of the spatial distribution of biogenic
309 volatile organic compound (*BVOC*) sources (isoprene, monoterpenes) on measured fluxes
310 (e.g., Spirig et al., 2005). The field measurements were supported by the physical modelling
311 of this forest site in a wind tunnel (Aubrun et al., 2005), also to estimate the influences of
312 spatial heterogeneity of emission sources on measured fluxes of some *BVOCs*.

313

314 During the ECHO campaign, a feasibility study was performed on 25 July (day 206 of year
315 2003) to measure fluxes and higher order moments (e.g., covariances) not only for isoprene
316 but also for the first time for *OH*- and *HO₂*- radicals. The data from these measurements were
317 analyzed in detail for the time period between 09:00 and 15:00 CET. This period was
318 characterized by cloudy conditions with a moderate horizontal wind velocity variation and
319 slightly unstable to neutral stratification above the canopy. Broken cloud fields caused
320 significant fluctuations of all radiation quantities above canopy. The air temperature, T_a , at
321 the measuring height $z_R = 37$ m increased from 19 to 26.5 °C, while the specific humidity,
322 q_a , increased only slightly from 09:00 to 12:00 CET from 8.3 $g\ kg^{-1}$ up to about 9.5 $g\ kg^{-1}$
323 and then decreased to about 8 $g\ kg^{-1}$ (Dlugi et al., 2010, 2014).

324

325 All measurements reported in the present paper were obtained at the main tower (Dlugi et al,
326 2010; 2014). The main tower with a height of 41 m, and the main measuring platform
327 at $z_R = 37$ m, was equipped with nine sonic anemometers/thermometers (METEK, instrument
328 type: USA-1; time resolution 10 Hz) between 2 m and 41 m, and eight psychrometers (dry
329 and wet bulb temperatures) at the same heights, except at 41 m. A time resolution for air
330 temperature, T_a , and specific humidity, q_a , of 15 s could be achieved. Radiation quantities
331 and photolysis frequencies were obtained by radiometers directly above the canopy ($h_c =$
332 30 m) with a time resolution of 3 s (Bohn et al., 2004; Bohn, 2006; Bohn et al., 2006).
333 Occasionally vertical profiles were measured.

334



335 The OH and HO_2 radical concentrations were measured by Laser Induced Fluorescence (LIF;
336 Holland et al., 1995, 2003) on a vertically movable platform. For the reported measurements
337 it was positioned above the canopy, with the inlet at 37 m height (Kleffmann et al., 2005). A
338 proton-transfer-reaction mass spectrometer (PTR-MS) for measurements of isoprene,
339 monoterpenes, methyl vinyl ketone (MVK), and methacrolein (MACR) was installed at the
340 ground, using a sampling line to collect air at the height of the ultrasonic anemometer
341 (Ammann et al., 2004; Spirig et al., 2005). The distances of the inlets of the PTR-MS and LIF
342 instruments from the ultrasonic anemometer measuring volume were 0.45 m and 0.6 m,
343 respectively. This spatial arrangement requires corrections to the calculated fluxes as
344 outlined by Dlugi et al. (2010) and Dlugi et al. (2014). The time series of OH (and HO_2) and
345 isoprene are available with a resolution of 0.2 Hz for the calculation of higher order mixed
346 moments (e.g., covariances).

347

348

349

350 2.2. ATTO 2015

351

352 The ATTO-IOP1 was conducted at the Amazon Tall Tower Observatory (Andreae et al.,
353 2015) in November 2015 (from 1 to 23 November) under El Niño conditions (Jiménez-Muñoz
354 et al., 2016; Wang and Hendon, 2017). Measurements were made on an 80 m walk up tower
355 at a height of $z_R = 41$ m. The average canopy height, h_c , in the surroundings of the tower is
356 around 35 m. The vertically integrated one-sided leaf area index (LAI) around the tower was
357 about 6. The land cover in the main wind direction is primary rain forest with an extension of
358 several hundred kilometers. During daytime, cumulus clouds develop regularly after noon.

359

360 Isoprene mixing ratios were measured by a PTR-MS at 1 Hz resolution. Air was drawn from
361 the measurement height (41 m) by a 3/8-inch opaque fluorinated ethylene propylene (FEP)
362 tubing at a rate of about 10 l min^{-1} . The line was isolated and heated. The inlet was protected
363 by a $5 \mu\text{m}$ pore size Teflon filter. The time delay of the measured signal was corrected by
364 maximizing the covariance between fluctuations of an open path H_2O analyzer (Licor 7500,
365 Licor, USA) in front of the inlet and the signal of the water clusters inside the PTR-MS.

366

367 Atmospheric OH and HO_2 were measured during 16 – 23 November 2015 using a modified
368 version of the HydrOxyl Radical measurement Unit based on fluorescence spectroscopy
369 (HORUS) instrument (Martinez et al., 2010; Hens et al., 2014). The laser system was
370 mounted on a cantilever balcony assembly at 36 m and the detection systems were mounted



371 on another cantilever balcony at 40 m along with instruments to measure radiation, isoprene,
372 and water vapour. The balcony faced to the north-east, the direction of the prevailing wind.

373

374 The measurements of atmospheric OH was achieved by measurements of the total OH
375 signal, i.e., the signal produced due to fluorescence at 308 nm of atmospheric OH as well as
376 of OH produced in the system during its travel time from the inlet nozzle to the detection
377 volume, which we call background OH . The difference between the total signal and the
378 background signal is thus a measure of atmospheric OH . The background OH can be
379 measured by scavenging of the atmospheric OH with propane. The propane was introduced
380 through an inlet pre-injector (IPI) mounted on top of the inlet nozzle (Novelli et al., 2014; Mao
381 et al., 2012; Hens et al., 2014). During previous campaigns using the IPI system, the
382 propane flow was switched on and off for two minutes each, providing a 4 minute time
383 resolution for measurements of atmospheric OH . For this campaign, we used an additional
384 detection unit for simultaneous measurements of total and background OH in order to
385 increase the time resolution of atmospheric OH measurements. The detection unit for
386 background OH was placed 55 cm to the east of the detection unit for total OH (Figure1).

387

388



389

390 **Fig. 1** Set up of instruments and HORUS- inlets at $z_R \approx 41$ m at the ATTO tower during ATTO 2015.
391 An inlet pre-injector is mounted on the inlet to the right side of the picture.

392

393 For measurement of HO_2 a second detection cell was mounted in series with the detection
394 cell for total OH (without propane addition). NO was added in between the measurement



395 cells to convert HO_2 to OH , which is then detected in the second cell (Hens et al., 2014;
396 Mallik et al., 2018).

397

398 The laser system consisted of a tunable dye laser which was pumped by a diode-pumped
399 Nd:YAG laser (Navigator I J40-X30SC-532Q, Spectra Physics) pulsing at 3 kHz. The 308 nm
400 output laser radiation was split in a 3:1:3 ratio using beam splitters, and channeled through 5
401 m optical fibers into the three detection cells to measure total OH , HO_2 and background OH .

402

403 Ambient air was drawn into the inlets through critical orifices with pinhole sizes of 0.9 mm
404 each into the respective detection cells below. The pinhole of the nozzles were 120 cm
405 above the platform base at 40 m above ground level and about 10 m above the canopy. The
406 internal pressure in the two OH detection cells, 4.5 ± 0.1 hPa, was maintained by two
407 separate but identical pump systems mounted below the tower and connected to the
408 respective detection systems by 50 m long (50 mm ID) tubes. The first pump system was
409 used to draw in air for the total OH and HO_2 measurements and the second one for
410 background OH .

411

412 The background OH was measured by titration with 12.5 cm^3 (STP) of pure propane in a
413 carrier flow of 7000 cm^3 (STP) synthetic air. The scavenger amount was just sufficient to
414 scavenge off ~95% of atmospheric OH as determined from propane titration experiments on-
415 site. Initially, IPI systems were mounted on top of both the detection units, to be able to
416 alternate measurements of total and background OH measurements between the two units
417 and characterize the losses occurring due to the IPI systems. The IPI systems were
418 connected to a blower via a t-piece and individual valves adjusted for a flow of about 140 lpm
419 of ambient air from the top of each IPI. The wall losses in the IPI were periodically
420 determined by physically dismounting the IPI for 5 minutes during measurements during
421 different times of the day.

422

423 For the measurement phase (19 - 23 Nov, 2015; day no: 323 (midday) - 327), the IPI was
424 mounted only on the detection unit for background OH , providing us with a high time
425 resolution for atmospheric OH measurements. In this phase, the scavenger was injected
426 continuously resulting in measurements of total OH and background OH at a high time
427 resolution of 15 s. The difference between these two signals gives a measure of the
428 atmospheric OH at the same time resolution.

429

430 Calibration of the instrument for OH and HO_2 measurements was achieved by measuring the
431 signals generated by known amounts of OH and HO_2 in a calibrator setup (Martinez et al.,



432 2010). The calibrator was mounted on top of the *OH* inlet without the IPI. Known amounts of
433 *OH* and *HO*₂ were produced by irradiating different concentrations of humidified air with 185
434 nm radiation produced by a pen ray Hg lamp. The actinic flux density of the Hg lamp (Pen-
435 ray line source, LOT-Oriel, Germany) used for the photolytic radical production was
436 determined before and after the campaign using the actinometry method by *N*₂*O* photolysis
437 (Martinez et al., 2010; Hens et al., 2014). The different *OH* and *HO*₂ mixing ratios were
438 produced by mixing different combinations of humidified and dry air flows using mass flow
439 controllers. The water mixing ratio in humid air stream was measured by a LICOR CO₂/H₂O-
440 Analyzer (Li-7000).

441

442

443

444 2.3. NOMADSS – Field Study 2013

445

446 The Nitrogen, Oxidants, Mercury and Aerosol Distributions, Source and Sinks (NOMADSS)
447 project was performed within the Southeast Atmosphere Study. NOMADSS consisted of
448 three projects, one was the Southern Oxidant and Aerosol Study (SOAS). The results
449 discussed by Kaser et al. (2015) are from flights conducted within SOAS by the National
450 Center for Atmospheric Research's C130 aircraft in June / July 2013 in the central and
451 southeast U.S. The complete planetary boundary layer budget of isoprene was measured
452 (Kaser et al., 2015). Within these studies also the intensity of segregation for the reaction
453 between isoprene and *OH* (Eq. (4)) was determined.

454

455 Isoprene was measured by a PTR-MS with a repetition rate of > 1 Hz, during research flights
456 RF13 and RF17. This time resolution is considered to be high enough to perform eddy
457 covariance calculations for the isoprene flux $\overline{w'c'_i}$ and the covariance $\overline{c'_i c'_j}$ in Eq. (1) (e.g., Karl
458 et al., 2013). In addition, a Trace Organic Gas Analyzer (TOGA) (e.g., Hornbrook et al, 2011)
459 was applied also for measuring isoprene mixing ratios with a time resolution of about 2
460 minutes.

461

462 The *HO*_x- radicals, *OH* and *HO*₂, were detected using an ion chemical ionization mass
463 spectrometer (Hornbrook et al, 2011; Mauldin III et al., 2003) as reported by Kaser et al.
464 (2015; in text S3 of the supplement). Data for “OH were collected every 30 seconds”, so that
465 a time resolution of 0.033 Hz was obtained. To generate *OH* data with higher time resolution
466 Kaser et al.,(2015) “used spectral similarity conditions to reconstruct the spectral high-
467 frequency loss based on concomitant fast isoprene and ozone measurements” both with time
468 resolutions of 1 s, up to 5 Hz sampling rate (see also Fig. S4 in Kaser et al., 2015).



469

470 In addition, observed and modelled isoprene surface fluxes were compared. The segregation
471 intensity was modelled by the LES- code described by Patton et al. (2003) with the chemistry
472 as given by Patton et al. (2001). Simulations were performed for homogeneous and
473 heterogeneous (or inhomogeneous) land surface conditions, also to compare to results given
474 by Ouwersloot et al. (2011).

475

476

477

478 3. Theoretical Concepts for Data Analysis

479

480 3.1. Introduction

481

482 Non-homogeneous mixing of chemically reactive compounds (i, j) causes a reduction of their
483 mean reaction rates, $\overline{R_{ij}} = k_{ij} \times \overline{c_i} \times \overline{c_j}$, derived for homogeneous mixed conditions. Here, k_{ij}
484 is the reaction rate constant, c_i, c_j are the specific mixing ratios, and the overbar denotes
485 time averaged mean values (e.g., Seinfeld and Pandis, 1997).

486

487 As discussed before, for a second order reaction the influence of non-homogeneous mixing
488 is commonly described by the intensity of segregation, I_s . This quantity is formulated in the
489 sense of Reynolds (1895) and extended by Richardson (1920) for compressible fluids with all
490 quantities α being a combination of their ensemble averages $\hat{\alpha}$ and the deviations $\tilde{\alpha}$ from
491 that $\hat{\alpha}$. Here we replace $\hat{\alpha}$ by their timely averaged means $\overline{\alpha}$ and $\tilde{\alpha}$ by the deviation α' from $\overline{\alpha}$
492 (see Monin and Yaglom, 1971; Sorbjan, 1989 or Higgins et al., 2013 for further discussion).
493 Therefore $\alpha = \overline{\alpha} + \alpha'$ and with the extension for mixing ratios, c_i and c_j , the reaction rate, R_{ij} ,
494 with the intensity of segregation, I_s , is given by (e.g., Astarita, 1967; O'Brien, 1971;
495 Danckwerts, 1952; Donaldson, 1975; Lamb and Seinfeld, 1973; Shu, 1976):

$$496 \quad R_{ij} = k_{ij} \times \overline{c_i} \times \overline{c_j} \left(1 + \frac{\overline{c_i'c_j'}}{\overline{c_i} \times \overline{c_j}} \right) = \overline{R_{ij}} (1 + I_s) \quad (1)$$

497 In general, a covariance $\overline{\alpha'\beta'}$ of two quantities α, β can be written as the product of the
498 related standard deviations, σ_α and σ_β , times the correlation coefficient, $r_{\alpha\beta}$. For c_i, c_j this
499 expression reads (Eq. (2))

$$500 \quad \overline{c_i'c_j'} = r_{ij} \times \sigma_i \times \sigma_j, \quad (2)$$

501 at least if both quantities have probability density functions comparable to normal or log-
502 normal distributions (Sachs and Hedderich, 2006). Combining Eq. (1) and Eq. (2) results in



503
$$I_s = r_{ij} \times \frac{\sigma_i \times \sigma_j}{c_i \times c_j} \quad (3)$$

504 with the covariance replaced by the product of terms on the right hand side of Eq. (2).

505 Here results only of reaction (4)



506 are discussed, i.e., between a secondary compound, c_i (OH), and a primary, emitted
 507 compound, c_j (ISO). The depletion of the reacting compounds in Eq. (4) results in an anti-
 508 correlation between c_i and c_j . Consequently the covariance (Eq. (1) - Eq. (2)) and the
 509 correlation coefficient, r_{ij} , (Eq. (2) - Eq. (3)) become negative, which results in $I_s \leq 0$ in Eq.
 510 (1) and Eq. (3). Therefore, the reaction rate, R_{ij} , in Eq. (1) will be smaller than in the
 511 homogeneously mixed case, $\overline{R_{ij}}$, as measured, e.g., under laboratory conditions to
 512 determine k_{ij} (e.g., Finlayson Pitts and Pitts, 1986).

513

514 Compounds like isoprene, but also other hydrocarbons, CO , CH_4 , NO , or NO_2 are mainly
 515 emitted near the surface of the Earth. Other reactive compounds like OH (but also $C_xH_yO_z$
 516 O_3) are produced in the volume of the atmosphere in the course of chemical cycling (e.g.,
 517 Seinfeld and Pandis, 1997; Rohrer et al., 2014).

518

519 In our discussion on the intercomparison of results from field and modelling studies for
 520 reaction Eq. (4) and of the influence of segregation, we have to analyze the multiple
 521 influences of the terms in Eq. (1) and Eq. (3) on I_s . Note that the turbulent vertical fluxes of
 522 compounds like c_i near the surface can be related to their emission rates (e.g., Guenther et
 523 al, 2006; Müller et al, 2008) at the surface E_i (e.g., from plants). E_{i0} is related to the turbulent
 524 surface flux $\overline{w'c_i}|_0 = E_{i0}$ and – in analogy to Eq. (2) – may be written as

525
$$E_{i0} \equiv \overline{w'c_i} = r_{wc_i} \times \sigma_w \times \sigma_i \quad (5)$$

526 with the vertical wind velocity component w . If one formally replaces the standard deviation
 527 σ_i (e.g., for isoprene) in Eq. (3) by σ_i from Eq. (5), a relation where I_s is expressed also as
 528 function of the turbulent flux of compound c_i (Eq. (6)) can be formulated.

529
$$I_s = \underbrace{\left(\frac{r_{ij}}{r_w}\right)}_1 \times \underbrace{\left(\frac{w'c_i}{\sigma_w \times c_i}\right)}_2 \times \underbrace{\left(\frac{\sigma_j}{c_j}\right)}_3 \quad (6)$$

530 Eq. (6) is composed of three terms:

531 (1) the ratio of the two correlation coefficients, (2) the ratio of the turbulent flux of compound
 532 c_i (here: ISO) and the product of the standard deviation of the vertical wind velocity
 533 component with the time average of the mixing ratio of c_i , and (3) the normalized standard



534 deviation of compound c_j (here: OH). All these quantities can be directly determined from
535 high frequency measurements (e.g., $\overline{c_i}$, $\overline{c_j}$, $\overline{c_i'c_j'}$, σ_i , σ_j , $\overline{w'c_i'}$, $\overline{w'c_j'}$, ...).

536

537 In models, prognostic (or balance) equations for any of these quantities (e.g., $\overline{c_i}$, $\overline{c_j}$, $\overline{c_i'c_j'}$, σ_i ,
538 σ_j , $\overline{w'c_i'}$, $\overline{w'c_j'}$, ...) are solved to predict their behavior in time and space and their interactions.

539 In this work, these quantities are calculated from direct measurements, or their order of
540 magnitude is estimated to be able to determine which processes in the turbulent, convective
541 atmospheric boundary layer (ABL) have the greatest influence on I_s .

542

543 Therefore, we need to consider how the I_s for reaction Eq. (4) could be related to the mean
544 mixing ratios and the fluxes of the reactants ($\overline{w'c_i'}$, $\overline{w'c_j'}$), the variances ($\overline{c_i'^2}$, $\overline{c_j'^2}$) or other
545 terms in the prognostic equations. We also need to briefly revisit the derivation of the
546 diagnostic equation for I_s given by Dlugi et al. (2014), in order to clarify if a relation between
547 the isoprene flux ($\overline{w'c_i'}$) and I_s can be established by the theoretical concept and to define
548 the conditions under which experimental findings might also show such a relationship, i.e., a
549 significant correlation between I_s and $\overline{w'c_i'}$. The following analysis is based on data from the
550 field studies ECHO 2003 and ATTO 2015 and is compared to modelling results by
551 Ouwersloot et al. (2011) and Patton et al. (2001) and also to findings described by Kaser et
552 al. (2015) from the NOMADSS campaign.

553

554 We will examine the second-order equations that describe basic physical and chemical
555 processes, which control the time behavior of the different input variables (mean mixing
556 ratios, variances, co-variances) of Eq. (1) and Eq. (3) that are used to determine the intensity
557 of segregation and finally the terms in the diagnostic equation for I_s itself. The product of the
558 mean mixing ratios is the denominator in Eq. (1) and Eq. (3). The balances of the mixing
559 ratios are described in the following section 3.2. The standard deviations (σ_i , σ_j) in Eq. (3) or
560 Eq. (5) are given by the square roots of the variances. In Section 3.3 we therefore discuss
561 which terms influence the variances of isoprene (or σ_i) and of OH . In Section 3.4 we also
562 estimate terms of the balance of $\overline{w'c_i'}$ (i.e., the isoprene flux) and their relationship to Eq. (6).
563 Finally various influences of different processes (chemistry and mixing) on the balance of I_s
564 are discussed in Section 3.5.

565

566

567

568 **3.2. Results for the Balance of the Mixing Ratios**



569

570 The balance of the mean mixing ratios, \bar{c}_i , \bar{c}_j , is commonly analyzed by the corresponding
571 prognostic equations (e.g., Stull, 1988). Here we shortly summarize the results discussed by
572 Dlugi et al. (2014) on the balance of $\bar{c}_i = ISO$ and (where needed) on $\bar{c}_j = OH$. The balance
573 for \bar{c}_i is given by

$$574 \quad S = \frac{\partial \bar{c}_i}{\partial t} = -\frac{\partial}{\partial x_k} \left(\underbrace{\overline{u_k \times \bar{c}_i}}_{DMF} + \underbrace{\overline{u'_k c'_i}}_{DTF} \right) - k_{ij} \left(\underbrace{\overline{c_i \times \bar{c}_j}}_{MR} + \underbrace{\overline{c'_i c'_j}}_{TR} \right) \quad (7)$$

575 with $(x_1, x_2, x_3) = (x, y, z)$ for the coordinate axes, $(u_1, u_2, u_3) = (x, y, z)$ for the wind velocity
576 components along these coordinate axes, and the other notation used as in Eq. (1) - Eq. (4).
577 In Eq. (7) as well as the following equations, Einstein's summation convention is used. Dlugi
578 et al. (2014) discussed the application of Eq. (7) for the ECHO 2003 study. The same
579 concept is applied for the analysis of ATTO 2015.

580

581 The range of numerical values for the first term of Eq. (7) – commonly named *storage term S*
582 - is given together with the computed results for *MR* and *TR* (*MR* = mean (time averaged)
583 reaction rate between both compounds and *TR* = reaction rate of correlated turbulent
584 fluctuating compounds (c'_i, c'_j)) together with the residuum given by *DMF* = divergence of the
585 advective flux with the mean flow ($\overline{u_k}$) and *DTF* = divergence of the turbulent flux ($\overline{u'_k c'_i}$) in
586 Table 1. Here k_{ij} is the reaction rate constant with an average value of $k_{ij} = 2.3 \text{ ppb}^{-1} \text{ s}^{-1}$ for
587 the reaction between isoprene and *OH* in the temperature range between 290 K and 300 K
588 for both field studies. An averaging time interval for both field studies (ECHO 2003, ATTO
589 2015) of 10 minutes is selected to always fulfil conditions of stationarity during cloudy
590 conditions at both field sites, as also discussed by Dlugi et al. (2010; 2014).

591

592 **Tab. 1** The range of magnitude for all terms of Eq. (7) for isoprene in ppb s^{-1} for ECHO (25 July 2003)
593 and ATTO (22 November 2015) with DMF+DTF determined as residuum.

Term	ECHO 2003	ATTO 2015
S	$(-0.8 \text{ to } 1.2) \cdot 10^{-3}$	$(-1.3 \text{ to } 6) \cdot 10^{-3}$
MR	$(1 \text{ to } 7) \cdot 10^{-4}$	$(1 \text{ to } 9.5) \cdot 10^{-4}$
TR	$(0 \text{ to } 7) \cdot 10^{-5}$	$(0 \text{ to } 8) \cdot 10^{-5}$
DMF +DTF	$(-0.5 \text{ to } 1.8) \cdot 10^{-3}$	$(-0.9 \text{ to } 7) \cdot 10^{-3}$

594

595 This analysis of data, for the isoprene balance from two field studies above the canopy top,
596 shows that the term *S* (Eq. (7)) is balanced mainly by the divergence of the fluxes with a
597 contribution of the mean reaction rate, *MR*, by about 10% or less and with $TR \leq 0.1 MR$



598 (Table 1). During ATTO 2015, turbulent flux measurements for isoprene at height $z_R = 41$ m
599 were performed. In addition, the related flux divergence is estimated based on
600 measurements during ECHO 2003 proportional to the measured vertical gradient of the
601 isoprene mixing ratio and the turbulent sensible heat flux divergence.

602

603 The term

$$604 \quad DMF = \overline{u_k} \times \frac{\partial \overline{c_i}}{\partial x_k} + \overline{c_i} \times \frac{\partial \overline{u_k}}{\partial x_k} \quad (8)$$

605 is either calculated as a residuum (Table 1) or it can be estimated from the measured values
606 at z_R and the vertical isoprene gradient. This latter method allows finding additional
607 controlling parameters for $\overline{c_i}$, $\overline{c_j}$. The upward directed vertical turbulent fluxes of isoprene
608 (emission flux) are in the range $0 < \overline{w'c'_i} < 0.3$ ppb m s⁻¹ (25 July 2003) for ECHO and
609 $0 < \overline{w'c'_i} < 1$ ppb m s⁻¹ (22 November 2015) for ATTO. Note that for a mean upward directed
610 vertical velocity $\overline{w} = 10^{-3}$ m s⁻¹ (e.g., Stull, 1988), the mean vertical advective flux is in the
611 range $10^{-3} \leq \overline{w} \cdot \overline{c_i} \leq 2 \cdot 10^{-2}$ ppb m s⁻¹ for ATTO and smaller by up to an order of
612 magnitude for ECHO. The accuracy of vertical velocity measurements during ECHO 2003 for
613 the METEK USA1 ultrasonic anemometer is about 0.005 m s⁻¹ (Dlugi et al., 2010; 2014) and
614 for ATTO 2015 (CSAT3) it is about 0.01 m s⁻¹. If \overline{w} reaches values above 0.1 m s⁻¹ - for
615 example during convective conditions - the fluxes with the mean flow become larger than the
616 turbulent fluxes. Such conditions were observed during the case study of ECHO 25 July,
617 2003 (Dlugi et al., 2014) and also during the ATTO experiment on 22 November, 2015.
618 Therefore, also the divergence of the mean flow (*DMF*) may be equal to or even larger than
619 the divergence by the turbulent components (*DTF*) in Table 1. Measured values of *DTF* for
620 isoprene from an aircraft campaign in California (different environment) are in the range of
621 $2 - 3 \cdot 10^{-4}$ ppb s⁻¹ with surface fluxes of the order of 0.3 ppb m s⁻¹ (Karl et al., 2013) while
622 Su et al. (2015) reported surface fluxes around 1 ppb m s⁻¹ in the NOMADSS area. Note that
623 the emission flux rate, E_{i0} , enters as the lower boundary condition if Eq. (7) is integrated
624 along the z-coordinate. E_{i0} represents the *surface flux*, $\overline{w'c'_i}|_0$, as $\overline{w} = 0$ at leaf surfaces (e.g.,
625 Kramm, 1995; Müller et al., 2008). The flux divergence and not the flux itself controls $\overline{c_i}$. The
626 sign of the divergence terms can be positive or negative. Therefore, only a change in
627 dynamic conditions from convergence to divergence in the wind field with constant E_{i0} may
628 significantly change S and potentially also MR and TR .

629

630 As a consequence, the surface flux, E_{i0} , the spatial distribution of the mean mixing ratios, $\overline{c_i}$
631 and $\overline{c_j}$, but also of wind velocity components, $(\overline{u}, \overline{v}, \overline{w})$, are important for the time behavior of
632 the mixing ratios in the atmosphere and near the canopy top. The balance of $\overline{c_j}$ above
633 canopy top is only given by the chemical sinks and sources because mixing and advection



634 on a spatial scale above 1 m^3 are not relevant for a compound with $\tau_c < 1\text{ s}$ and the terms
635 *DMF* and *DTF* are zero. But compounds influencing the production or consumption of *OH* are
636 advected to the measuring point and influence the magnitude and variability of *S*, *MR*, and
637 *TR*.

638

639 Additionally, the segregation intensity, I_s , (Eq. (3)) is influenced by the standard deviations σ_i
640 and σ_j . Patton et al. (2001) referred to the scalar variance budget and showed that second
641 order reactions may act to destroy, but also to produce, variance of isoprene ($\sigma_i^2 = \overline{c_i'^2}$). We
642 will therefore also discuss the balance of the variance in the following section 3.3.

643

644

645

646 3.3. Results for the Balance of the Variance

647

648 The analysis of terms of the balance equation of the covariance $\overline{c_i'c_j'}$ calculated from
649 measurements during ECHO 2003 suggests that the normalized variance of isoprene can
650 significantly influence I_s for the reaction of isoprene with *OH* (Dlugi et al., 2014). This agrees
651 with earlier results of Patton et al. (2001) from LES modelling for an idealized forest, and,
652 therefore, needs further consideration. Vinuesa and Vila-Guerau de Arellano (2005)
653 introduced diagnostic equations for the variance of reactants in a CBL model and
654 successfully predicted I_s as function of height for a reaction according Eq. (4). The balance
655 equation for the variance of c_i - here for a divergence free wind field for simplification - reads
656 (e.g., Stull, 1988, Sorbjan, 1989)

$$657 \underbrace{\frac{\partial}{\partial t} \overline{c_i'^2}}_{S_{var}} + \underbrace{\overline{u_k} \times \frac{\partial}{\partial x_k} \overline{c_i'^2}}_{A_{var}} + 2 \times \underbrace{\overline{u_k' \cdot c_i'} \times \frac{\partial}{\partial x_k} \overline{c_i'}}_{GP_{var}} + \underbrace{\frac{\partial}{\partial x_k} \overline{u_k' \cdot c_i'^2}}_{TT_{var}} + R_{var} + 2\varepsilon_{var} = 0 \quad (9)$$

658 The first term denotes local storage of variance (S_{var}), the second term describes advection
659 of spatial gradients of variance by the mean wind (A_{var}) while the third term is a production
660 term caused by turbulent motions (turbulent fluxes of c_i) in a field with a mean gradient of $\overline{c_i}$
661 and is often called gradient production term (GP_{var}). Term four describes the turbulent
662 transport of variance (TT_{var}), term five the chemical reactions (R_{var}) (see Eq. (10)) and term
663 six is molecular dissipation (ε_{var}). The analyses of Schaub (2007), Aubrun et al. (2005), and
664 Spirig et al. (2005) suggest that during ECHO 2003, isoprene is at least partly advected to
665 the main tower from nearby trees (see also: Dlugi et al., 2014). Therefore, for the ECHO
666 2003 case, horizontal and vertical advection by the mean wind field, as described by the
667 second term, A_{var} , may have significantly influenced the local mixing ratio $\overline{c_i}$ and the
668 variance.



669

670 It was shown by model calculations by Schumann (1989), Patton et al. (2001), and Vinuesa
 671 and Vila-Guerau de Arellano (2005) that chemical reaction terms may be as large as other
 672 dynamic terms. The reaction term R_{var} in Eq. (10) reads

673

$$674 \quad R_{var} = -2k_{ij} \left(\frac{\overline{c_i'^2} \times \overline{c_j}}{I} + \frac{\overline{c_i'c_j'} \times \overline{c_i}}{II} + \frac{\overline{c_i'c_i'c_j'}}{III} \right) + J \times \overline{c_i'c_j'} \quad (10)$$

675 if a reversible reaction $c_i + c_j \rightarrow c_k$ (e.g., by photolysis of a product c_k with photolysis rate J)
 676 is possible. The fourth term in Eq. (10) does not apply for a reaction like $OH + isoprene$.

677

678 If stationarity conditions ($S_{var} = 0$) are considered, according to the experimental findings,
 679 which showed that this term sometimes is much smaller than others, another relation is given
 680 by the combination of Eq. (9) and Eq. (10). In such case the variance $\overline{c_i'^2}$ (occurring in term I
 681 of R_{var}) can be related to the sum of all other terms in a diagnostic form by

$$682 \quad \overline{c_i'^2} = \frac{1}{k_{ij} \overline{c_j}} \left[\frac{\overline{u_k'c_i'} \times \frac{\partial}{\partial x_k} \overline{c_i}}{GP_{var}} + \frac{1}{2} \overline{u_k} \times \frac{\partial}{\partial x_k} \overline{c_i'^2} + \frac{1}{2} \frac{\partial}{\partial x_k} \overline{u_k'c_i'^2} + \varepsilon_{var} - k_{ij} \left(\frac{\overline{c_i} \times \overline{c_i'c_j'}}{II} + \frac{\overline{c_i'c_i'c_j'}}{III} \right) \right] \quad (11a)$$

683 A form for the vertical coordinate (z) only reads

$$684 \quad \overline{c_i'^2} = \frac{1}{k_{ij} \overline{c_j}} \left[\frac{\overline{w'c_i'} \times \frac{\partial}{\partial z} \overline{c_i}}{GP_{z,var}} + \frac{1}{2} \overline{w} \times \frac{\partial}{\partial z} \overline{c_i'^2} + \frac{1}{2} \frac{\partial}{\partial z} \overline{w'c_i'^2} + \varepsilon_{var} - k_{ij} \left(\frac{\overline{c_i} \times \overline{c_i'c_j'}}{II} + \frac{\overline{c_i'c_i'c_j'}}{III} \right) \right] \quad (11b)$$

685 In Eq. (6) the standard deviation for isoprene $\sigma_i = (\overline{c_i'^2})^{1/2}$ is replaced by $\overline{w'c_i'} \cdot (\overline{r_{wc_i}} \cdot \sigma_w)^{-1}$
 686 according to Eq. (5) to formally relate I_s to the turbulent isoprene flux. Here the variance is
 687 related in an additive form to the turbulent flux in GP_{var} and to the covariance $\overline{c_i'c_j'}$ in I_s (Eq.
 688 (1)) by term II . Note that for a non-reactive scalar with $R_{var} = 0$ such diagnostic relations
 689 (Eq. (11a), Eq. (11b)) cannot be derived!

690

691 An order of magnitude estimation can be performed for all terms in Eq. (9), Eq. (11a), and
 692 Eq. (11b) to quantify which terms may have the largest impact on the variance. This
 693 calculation is based on results given by Dlugi et al. (2010, 2014) for ECHO 2003 and
 694 provided by Nölscher et al. (2016), Yanez-Serrano et al. (2015), and our own measurements
 695 (Section 2) for ATTO 2015 (Table 2).

696 1. The term $(k_{ij} \times \overline{c_j})^{-1}$ is the chemical reaction time scale, τ_c , (with the average
 697 $k_{ij} = 2.3 \text{ ppb}^{-1} \text{ s}^{-1}$; see section 3.2). For reaction Eq. (4) with $10^{-5} \leq [OH] \leq$
 698 $5 \cdot 10^{-4} \text{ ppb}$ this term is in a range of about 43.200 s (12h) to 650 s (0.18h). R_{var} (Eq.



699 (9) is not larger than $10^{-3} \text{ ppb}^2 \text{ s}^{-1}$ for ECHO 2003 and $3 \cdot 10^{-4} \text{ ppb}^2 \text{ s}^{-1}$ for ATTO
700 2015 (22 November). On average the terms in Table 2 have to be multiplied by
701 $(k_{ij} \times \bar{c}_j)^{-1} \approx 900 \text{ s}$ for ECHO 2003 and by 1900 s for ATTO 2015.

702

703 2. The term GP_{var} is the product of the turbulent flux components and the spatial
704 gradients of the mean isoprene mixing ratio, \bar{c}_i . The upward directed vertical turbulent
705 fluxes of isoprene are in the range $0.02 \text{ ppb m s}^{-1}$ to 0.6 ppb m s^{-1} (ECHO 2003) and
706 0 ppb m s^{-1} to 1 ppb m s^{-1} (ATTO; 22 November 2015). The measured vertical
707 gradients of isoprene at the ECHO site are 0.01 ppb m^{-1} to 0.05 ppb m^{-1} and at the
708 ATTO site 0.01 ppb m^{-1} to 0.07 ppb m^{-1} both for 10:00 – 16:00 LT and upward
709 directed fluxes (see also: Nölscher et al., 2015; Yanez-Serrano et al., 2015). Note
710 that large fluxes are sometimes also related to smaller gradients and smaller fluxes to
711 larger gradients. Therefore a range of $8 \cdot 10^{-4} \leq GP_{var} \leq 10^{-3} \text{ ppb}^2 \text{ s}^{-1}$ for ECHO
712 2003 and of $10^{-3} \leq GP_{var} \leq 3 \cdot 10^{-3} \text{ ppb}^2 \text{ s}^{-1}$ for ATTO 2015 (November 22) is
713 estimated.

714

715 3. For ECHO 2003, lateral and vertical advection of the isoprene mixing ratio \bar{c}_i (*DMF*
716 and *DTF*) are calculated to estimate the divergence of the fluxes in Eq. (7) (Table 1
717 and Dlugi et al., 2014). On average, the variance is $\overline{c_i'^2} \cong 0.42 \text{ ppb}^2$ and only larger
718 by about 10% for increasing isoprene mixing ratios caused by horizontal advection as
719 discussed by Dlugi et al. (2014). Vertical advection decreased \bar{c}_i to $\bar{c}_i < 0.4 \text{ ppb}$ but
720 also decreased the variance to an average of $\overline{c_i'^2} \cong 0.13 \text{ ppb}^2$ in the downward
721 transported air mass. With the average surface value being $\overline{c_i^2} = 0.42 \text{ ppb}^2$ and the
722 value in the overlying part of ABL being $\overline{c_i'^2} = 0.13 \text{ ppb}^2$, we estimate the origin of
723 these air volumes to be around 300 – 400 m above ground (calculated from the
724 difference in specific humidity and temperature). For an average $\bar{w} = -0.4 \text{ m s}^{-1}$
725 from measurements for these conditions, this term reaches values of about $A_{z,var} \cong$
726 $4.5 \cdot 10^{-4} \text{ ppb}^2 \text{ s}^{-1}$ for the ECHO 2003 case.

727

728 For ATTO we obtain $\overline{c_i'^2} \approx 5.2 \text{ ppb}^2$ ($\bar{\sigma}_i \approx 2.5 \text{ ppb}$) for mean mixing ratios $\bar{c}_i \approx 7 \text{ ppb}$
729 after noon with comparable \bar{w} and percentage changes of variance during
730 downdrafts. Therefore, this term is estimated to be of the same magnitude during
731 ATTO 2015 as for ECHO 2003. The horizontal advection term for ECHO 2003 can be
732 estimated with $\overline{u_H} = 2 \text{ m s}^{-1}$ and $\Delta \overline{c_i'^2} \cong 0.04 \text{ ppb}^2$ from measurements at a distance
733 of about 125 m between the west tower and the main tower (Dlugi et al., 2010; 2014)



734 to be $A_{h,var} \cong 8 \cdot 10^{-4} ppb^2 s^{-1}$. The observed change of variance during horizontal
 735 advection for ECHO 2003 is small. If we assume comparable conditions for the ATTO
 736 field site a magnitude of the horizontal advection of $A_{h,var} \approx 10^{-3} ppb^2 s^{-1}$ is
 737 determined.

738

739 For ECHO 2003, the vertical turbulent transport of isoprene variance is calculated
 740 from measurements as $\overline{w'c_i'^2} \leq 10^{-2} ppb^2 m s^{-1}$. The analysis of terms of the
 741 variance balance equations for potential temperature and of isoprene on day 200 –
 742 206 of ECHO 2003 shows, that TT_{var} for both quantities θ and ISO are proportional to
 743 each other. We assume that the percentage vertical change of TT_{var} is comparable to
 744 the change of the same term for temperature variance also on day 206 (25 July
 745 2003), when the ECHO 2003 case study on segregation (Dlugi et al., 2010; 2014)
 746 was performed, and obtain $TT_{var} \approx 5 \cdot 10^{-4} ppb^2 s^{-1}$. With the same relation we
 747 estimate $TT_{var} < 10^{-3} ppb^2 s^{-1}$ for ATTO 2015 (25 November 2015).

748

749 4. For the ECHO 2003 case the covariance in term *II* (Eq. 11a, 11b) is in the range
 750 $0 < \overline{c_i'c_j'} < 3 \cdot 10^{-5} ppb^2$ (see also Fig. 12 in Section 4.2.1 and Fig. 8 in Dlugi et al.,
 751 2014) with the average mixing ratio $\overline{c_i} \approx 0.7 ppb$. Therefore, for the ECHO 2003
 752 study, term *II* is smaller than $2 \cdot 10^{-5} ppb^2 s^{-1}$ and term *III* is $< 10^{-6} ppb^2 s^{-1}$ (see
 753 also Fig. 12 in Dlugi et al., 2014). Both terms are comparable in magnitude during
 754 ATTO 2015 (November 22, 2015). Table 2 summarizes these estimates.

755

756 5. Molecular dissipation (Sorbjan, 1989) is often determined by

$$757 \quad \varepsilon_\alpha = \nu_\alpha \overline{\left(\frac{\partial \alpha'}{\partial x_k}\right)^2}$$

758 for any quantity α (ν_α = kinematic molecular diffusivity for α in air). For the ECHO
 759 2003 case and for $\alpha \equiv c_i = ISO$, the kinematic molecular diffusivity is of order
 760 $10^{-5} m^2 s^{-1}$ and the gradient of fluctuations is about $10^{-2} ppb m^{-1}$ from
 761 measurements on days 200 – 203, 2003 (see above) (Dlugi et al., 2014). Therefore,
 762 an order of magnitude estimate is $\varepsilon_{var} \approx 10^{-9} ppb^2 s^{-1}$. Even for a gradient 10^2 times
 763 larger (e.g., of about $1 ppb m^{-1}$), we get $\varepsilon_{var} < 10^{-4} ppb^2 s^{-1}$.

764

765 These results show that conditions exist above canopy top where the *gradient*
 766 *production*, GP_{var} , becomes the largest term in the variance balance. Then the
 767 magnitude of $\overline{c_i'^2}$ is mainly determined by GP_{var} but with some significant contribution
 768 of variance advection A_{var} and TT_{var} (see Table 2), if Eq. (11a), Eq. (11b) are



769 approximately valid. In Section 4, we will discuss these findings together with the
770 question if I_s can be simply expressed by a proportionality to the turbulent isoprene
771 flux, $\overline{w'c'_i}$.

772

773 **Tab. 2** The estimation for the magnitude of terms in the diagnostic equations (Eqs. 11a, 11b) for the
774 isoprene variance during ECHO 2003 (25 July, 2003) and ATTO 2015 (25 November, 2015) in
775 [$\text{ppb}^2 \text{s}^{-1}$].

776

Term	ECHO 2003	ATTO 2015
GP_{var}	$8 \cdot 10^{-4}$ to 10^{-3}	10^{-3} to $3 \cdot 10^{-3}$
$A_{h,var}$	$\approx 8 \cdot 10^{-4}$	assumed to be $\approx 10^{-3}$
$A_{z,var}$	$\approx 4.5 \cdot 10^{-4}$	$\approx 4.5 \cdot 10^{-4}$
TT_{var}	$\approx 5 \cdot 10^{-4}$	assumed to be $< 10^{-3}$ (see text)
II	$\leq 4 \cdot 10^{-5}$	$\leq 4 \cdot 10^{-5}$
III	$\leq 10^{-6}$	$\leq 10^{-6}$

777

778

779

780 3.4. Results for the Balance of the Isoprene Flux

781

782 The balance of the isoprene flux is discussed in comparison to experimental results from the
783 field (ECHO 2003: Dlugi et al., 2010, 2014; ATTO 2015: see also Section 4). As an example,
784 we mainly focus on results from the ECHO 2003 campaign but also refer to ATTO 2015.

785

786 The vertical turbulent fluxes of reactive compounds like isoprene (*ISO*) and *OH* varied with
787 time during 25.07.2003 (DOY 206) of ECHO 2003 (Dlugi et al., 2010). Eq. (12) describes the
788 behavior of the vertical flux (without the influence of advection with the mean flow velocity)
789 for a component i and has different terms besides the reaction term R_{wi} (e.g., Patton et al.,
790 2001, Verver et al., 2000).

$$791 \quad \frac{\partial}{\partial t} \overline{w'c'_i} = \underbrace{-\overline{w'^2} \times \frac{\partial \overline{c_i}}{\partial z}}_i + \underbrace{\frac{g}{\theta_{v0}} \times \overline{c'_i \theta'_v}}_{ii} - \underbrace{\frac{\partial}{\partial z} \overline{c'_i w' w'}}_{iii} - \underbrace{\frac{1}{\rho} \times c'_i \frac{\partial p'}{\partial z}}_{iv} + \underbrace{R_{wi}}_v - \underbrace{2\varepsilon_{wi}}_{vi} \quad (12)$$

$$792 \quad R_i = -k_{ij} \left(\underbrace{\overline{c_i} \times \overline{w'c'_j}}_i + \underbrace{\overline{c_j} \times \overline{w'c'_i}}_{ii} + \underbrace{\overline{w'c'_i c'_j}}_{iii} \right) \quad (13)$$



793 Here, g is the acceleration of gravity, θ_v is the virtual potential temperature, p is the air
794 pressure. The reaction term in Eq. (13) is composed of the product of mean mixing ratios
795 with vertical fluxes (I : of OH ; II of ISO) and of the turbulent transport of the covariance – the
796 numerator of I_s of both reactants (see Eq. 1). All terms in Eq. (13) can be calculated from
797 measurements, while the other terms in Eq. (12) can be estimated as discussed in the
798 following.

799

800 For the reaction $ISO + OH$ (Eq. 4) the following order of magnitude estimation for terms in Eq.
801 (13) shows that most terms cannot be neglected a priori.

802

803 - The first term (I) in Eq. (13) is the product of the mean concentration of isoprene (in
804 the range of $0.1 - 2.5 \text{ ppb}$ for ECHO 2003 and $0.3 - 18 \text{ ppb}$ for ATTO 2015 (Section
805 2) with the turbulent flux of OH (in the range of about $10^{-5} - 5 \cdot 10^{-5} \text{ ppb m s}^{-1}$) for
806 both field experiments. The turbulent OH flux is often set to zero (e.g., Kaser et al.,
807 2015), although the numerical value is significant. This flux is the result of the in-flux
808 and out-flux of other chemical compounds which act as sinks and sources in a small
809 volume of the order $< 1 \text{ m}^3$ where the OH radical is locally detected. Due to its short
810 lifetime ($< 1 \text{ sec}$) OH is just transported on scales of a few centimeters. Considering a
811 mean value of $k_{ij} = 2.3 \text{ ppb}^{-1} \text{ s}^{-1}$ for reaction Eq. (4) this first term (I) varies in a
812 range of $4 \cdot 10^{-6} - 2.3 \cdot 10^{-3} \text{ ppb m s}^{-2}$.

813

814 - The mean OH mixing ratio for ECHO 2003 is between about 10^{-4} ppb and $5 \cdot$
815 10^{-4} ppb (with higher values up to $7 \cdot 10^{-4} \text{ ppb}$) and the turbulent isoprene flux varies
816 between about $0.02 \text{ ppb m s}^{-1}$ and 0.6 ppb m s^{-1} (Spirig et al., 2005; Dlugi et al.,
817 2010). This results in $10^{-6} \text{ ppb m s}^{-2}$ to $4.2 \cdot 10^{-5} \text{ ppb m s}^{-2}$ for the second term (II)
818 in Eq. (13). This result is comparable to the ATTO 2015 case. The turbulent isoprene
819 fluxes from other field studies are comparable in magnitude (e.g., Eerdeken et al.
820 2009).

821

822 - The third term (III), the turbulent transport of the numerator of I_s (e.g., Dlugi et al.,
823 2014), is of order of $6 \cdot 10^{-5} \text{ ppb m s}^{-1}$. This is in the upper range ($6 \cdot 10^{-6} -$
824 $6 \cdot 10^{-5} \text{ ppb m s}^{-2}$) of the second term and within the lower part of the range of the
825 first term. These findings will be discussed again when the storage term on the left
826 side of Eq. (12) and R_{wi} are compared.

827

828



829 In the balance equation for the determination of the flux of isoprene (Eq. (12)) the first term
830 on the right side (*i*) is composed of the vertical gradient and the variance of the vertical
831 velocity component w .

832

833 - Taking results from the vertical gradients of isoprene at the ECHO site (e.g., Schaub,
834 2007; Ammann et al., 2004), the gradients vary in the range $0.01 - 0.25 \text{ ppb m}^{-1}$
835 while the average variance of w is about $0.25 \text{ m}^2 \text{ s}^{-2}$.

836 This results in $2.5 \cdot 10^{-3} - 6.2 \cdot 10^{-2} \text{ ppb m s}^{-2}$ for this term (*i*) commonly named
837 *production of the isoprene* flux when there is a momentum flux in a flow field with a
838 mean isoprene gradient. This movement across a vertical gradient of c_i is related to
839 fluctuations in w as well as in c_i .

840

841 - The second term on the right (*ii*) relates the correlation between isoprene and vertical
842 potential temperature to convective up- or downdrafts. For $\theta_v > T(K)$ the covariance
843 varies between 0.02 ppb K and 0.2 ppb K (Dlugi et al., 2010). The quotient (g/θ_{v0}) is
844 on average $(9.8/295) \text{ K m s}^{-2}$. Therefore, the second term (*ii*) on the right side of Eq.
845 (12) is in the range $6 \cdot 10^{-4} - 6.6 \cdot 10^{-3} \text{ ppb m s}^{-2}$. For these conditions, term one (*i*)
846 is larger than or equal to term two (*ii*).

847

848 - The third (*iii*) and the fourth (*iv*) terms on the right side of Eq. (12) cannot be
849 calculated directly, because the corresponding measurements during ECHO 2003
850 and ATTO 2015 were performed only at one height, and, therefore, a vertical profile
851 for the turbulent diffusion term of the flux is only available from the ECHO experiment
852 on some days (see section 3.3), as also described by Dlugi et al. (2010, 2014). In
853 addition, high frequency pressure fluctuations are not measured directly. Both terms
854 can only be estimated based on measurements of the transport of heat, humidity, and
855 CO_2 from studies on other days at the ECHO site (Section 3.3). The turbulent
856 transport term (*iii*) itself is calculated from measurements (ECHO) for a height
857 interval between 42 m and 28 m (with the main measuring height at $z_R = 37 \text{ m}$ (see
858 Section 2.1)) and is of the order of $10^{-4} \text{ ppb m}^2 \text{ s}^{-2}$. Compared to the turbulent
859 transports of the heat flux and the turbulent kinetic energy from ECHO 2003 and
860 other studies (e.g., Raupach, 1988; Raupach et al., 1996), the vertical gradient of the
861 turbulent transport of isoprene is estimated to be of the order of
862 $3 \cdot 10^{-6} \text{ to } 10^{-5} \text{ ppb m s}^{-2}$. This is significantly smaller than the first and second term
863 of Eq. (12).

864



865 - The term (iv) is the most complicated to estimate. It redistributes c'_i within a volume
866 and may be replaced by $1/\bar{\rho} \times \overline{p'(\partial c'/\partial z)}$ if – as commonly done – $\overline{p'c'_i}$ is assumed
867 to be zero (e.g., Wyngaard, 1982). There are no experimental data available justifying
868 such assumption. Therefore, problems exist quantifying this term by its theoretical
869 derivation and the assumptions made to simplify the original term (e.g., Stull, 1988,
870 Sorbjan, 1989) as well as by the experimental difficulties related to determine reliable
871 values of p' . Here, two different approaches are applied to estimate the magnitude of
872 this term. The first applies measurements of $\partial c'_i/\partial z$ and combines them with data on
873 p' from literature.

874
875 Different measurements of p' in canopies (e.g., Launder, 1978; Wyngaard, 1982;
876 Shaw et al., 1990) showed that pressure fluctuations between about 0.1 – 15 Pa are
877 detected compared to mean values $\bar{p} \approx 1000 \text{ hPa}$. The mixing ratio fluctuations, c'_i ,
878 are in the range of about 0.1 ppb for ECHO 2003. For ATTO 2015 short time
879 fluctuations of the isoprene mixing ratio larger by up to a factor of 15 are detected.
880 This results for ECHO 2003 in values below $5 \cdot 10^{-4} \text{ ppb m s}^{-1}$ if a maximum
881 correlation coefficient $|r_{p\partial c}| = 0.6$ between p' and $\partial c'_i/\partial z$ as also given for
882 momentum transfer for r_{uw} is assumed (Kaimal and Finnigan, 1994). For ECHO 2003
883 this term (iv) is estimated in the range of numerical values ($< 10^{-4} \text{ ppb m s}^{-1}$) for the
884 turbulent transport term (iii) (e.g., Stull, 1988; Sorbjan, 1989). For ATTO 2015, this
885 term is larger, but $\leq 7 \cdot 10^{-4} \text{ ppb m s}^{-1}$.

886
887 The second approach applies an expansion by Launder (1978), using the Poisson
888 equation for $1/\bar{\rho} \times \overline{p'(\partial c'/\partial z)}$, which relates this term to a sum of three terms with the
889 dominant term given by $a_1 \cdot (\overline{w'c'_i}/\tau)$ with the closure constant in the range $2.5 \leq$
890 $a_1 \leq 5.0$ (Lang and Bradley, 1983). Here the time scale τ is used according to the
891 mixing length concept evaluated by Poggi et al. (2004) and applied by Cava et al.
892 (2006) for measuring heights $z/h_c > 0.75$ with $a_1 = 2.9$. This approach results in a
893 range of 10^{-3} to $5 \cdot 10^{-3} \text{ ppb m s}^{-1}$ and is up to one order of magnitude larger than
894 the result obtained by the first approach.

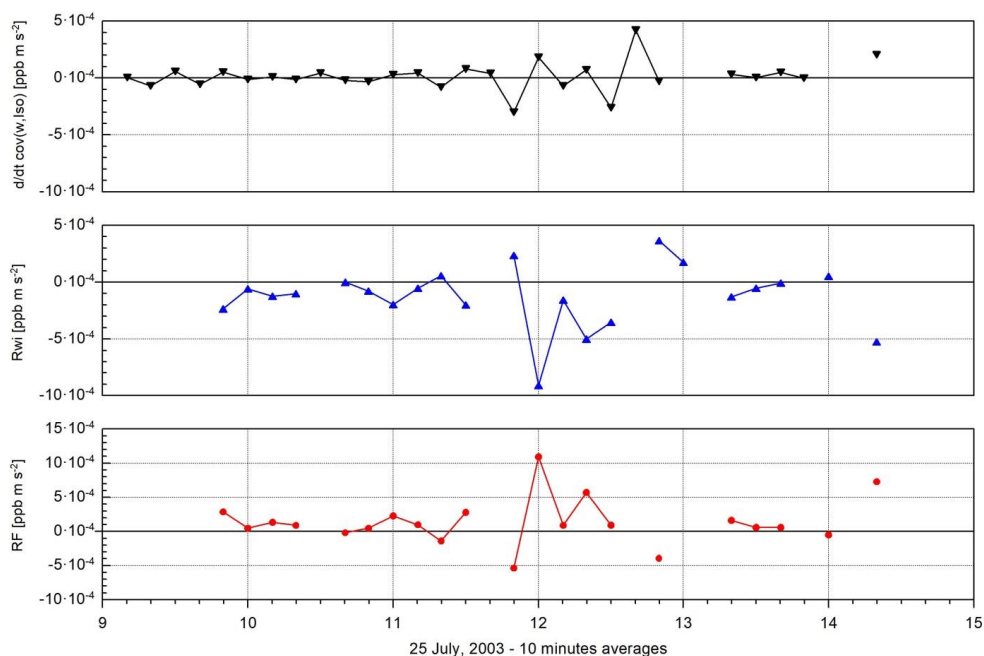
895
896 - The dissipation term ε_{wc} (vi) can be estimated according to Stull (1988) from the
897 covariance of gradients of w' and c' times the sum of kinematic molecular
898 diffusivities. This results in $\varepsilon_{wc} \leq 6 \cdot 10^{-8} \text{ ppb m s}^{-1}$ for the data sets applied by Dlugi
899 et al. (2014). Therefore, this term is smaller than the other terms in the air volume
900 above canopy top.



901

902 The storage term S_{wi} is directly calculated from field data (Fig. 2). As a result, the storage
903 term S_{wi} on the left side of Eq. (12) is comparable in magnitude to R_{wi} and the residuum RF
904 composed of all terms $(i) - (vi)$ on the right side without R_{wi} (see Fig. 2).

905



906

907 **Fig. 2** The storage term of the balance of the flux, the chemical reaction term R_{wi} , and the residuum,
908 RF , (see text) in Eq. (12) for the conditions during ECHO 2003 (25.07.2003) at height
909 $z_R = 37 \text{ m}$ at the main tower.

910

911

912 A net balance exists with $S_{wi} = RF + R_{wi}$ for the isoprene flux. Often S_{wi} is small compared to
913 the other terms, which compensate each other. But for convective conditions during 25 July
914 2003, between 11 – 13 CET, S_{wi} becomes comparable in magnitude to the other terms (e.g.,
915 Dlugi et al., 2014). Therefore, even if advection with the mean flow is not discussed here, the
916 influence of turbulent and convective transport and mixing expressed by term RF is
917 comparable to R_{wi} in magnitude. The role of term (vi) remains uncertain as long as an
918 evaluation of the Launder (1978) expansion for isoprene is missing, as it was done for heat
919 and moisture by Lang and Bradley (1983).

920



921 Note that Eq. (12) describes the variability with time of the isoprene flux, $\overline{w'c'_i}$. If we assume
 922 that S_{wi} is always smaller than other terms – e.g., neglect some larger values in Fig. 2 and
 923 use $S_{wi} \equiv 0$ – a diagnostic equation can be formulated as an estimate for $\overline{w'c'_i}$.

$$924 \quad \overline{w'c'_i} = \frac{1}{k_{ij} \cdot \overline{c'_j}} RF - \frac{\overline{c'_i}}{\overline{c'_j}} \times \overline{w'c'_j} - \frac{1}{\overline{c'_j}} \times \overline{w'c'_i c'_j}. \quad (14)$$

925 As mentioned above the flux $\overline{w'c'_j}$ is often assumed to be zero. In this case the flux of
 926 isoprene would be determined by RF (= sum of four terms (i) - (iv)) and term (v) in Eq. (12)
 927 multiplied by $\tau_c = (k_{ij} \cdot \overline{c'_j})^{-1}$, the chemical time scale for this reaction (e.g., Patton et al.,
 928 2001; Finlayson-Pitts and Pitts Jr., 1986) if term (I) in Eq. (13) can be neglected as
 929 discussed above. Therefore, a direct relationship between $\overline{w'c'_i}$ and $\overline{c'_i c'_j}$ or even with I_s is not
 930 given by Eq. (12) or Eq. (14), but a relation with the turbulent transport of the covariance
 931 ($\overline{w'c'_i c'_j}$) or with the four terms in RF can be established by Eq. (14).

932

933

934

935 3.5. The Balance of the Segregation Intensity

936

937 A diagnostic balance equation for I_s was described and discussed by Dlugi et al. (2014).
 938 Their analysis is based on the balance equation of the covariance $\overline{c'_i c'_j}$ which is the
 939 numerator in Eq. (1) for I_s . A short summary of this concept is given in the following. This
 940 balance equation reads:

$$941 \quad S_{cov} = \frac{\partial}{\partial t} \overline{c'_i c'_j} = -TPI_k - TPOH_k - A_{1k} - A_{2k} - TT_k - D + R_{ij} \quad (15)$$

942 with the *residual term RES* (see Eq. (10) in Dlugi et al., 2014)

$$943 \quad -RES = -TPI_k - TPOH_k - A_{1k} - A_{2k} - TT_k - D \quad (16)$$

944 S_{cov} is the storage term; TPI_k is the turbulent production by a turbulent flux of *isoprene* in a
 945 spatially inhomogeneous field of *OH*. $TPOH_k$ is the turbulent production by a turbulent flux of
 946 *OH* in a spatially inhomogeneous field of isoprene. As mentioned above, the turbulent fluxes
 947 of *OH* ($\overline{w'OH'}$, along the z - coordinate) are solely caused by the influence of chemical
 948 sources P_{OH} and sinks L_{OH} of *OH* (Dlugi et al., 2010; 2014), because *OH* has a chemical *life-*
 949 *time* $\tau_{OH} < 1$ s and is not transported above a spatial scale of one meter or so in the
 950 atmosphere. A_{1k} is the advection of covariance by the influence of the divergence of the flow
 951 field; A_{2k} is the advection of covariance with the mean flow; TT_k is the turbulent transport of
 952 the covariance $\overline{c'_i c'_j}$; D is the molecular diffusion term and R_{ij} the chemical reaction term.

953

954 The magnitude of



- 955 - D is generally below $10^{-8} \text{ ppb}^2 \text{ s}^{-1}$ and
 956 - S_{cov} is found experimentally to be below $6 \cdot 10^{-8} \text{ ppb}^2 \text{ s}^{-1}$,
 957 - while all other terms are in the range $10^{-6} \text{ ppb s}^{-1} \leq \text{terms} \leq 4 \cdot 10^{-4} \text{ ppb s}^{-1}$ (see
 958 also Table 3 in Dlugi et al., 2014).

959

960 For the reaction (Eq. (4)) ($ISO + OH$) during the ECHO 2003 and ATTO 2015 field studies the
 961 storage S_{cov} on the left side of Eq. (15) is significantly smaller than the other terms.

962 Therefore, stationarity conditions ($S_{cov} = 0$) can be applied and Eq. (15) reads

$$963 \quad RES = R_{ij} \quad (17)$$

$$964 \quad \text{with} \quad R_{ij} = -k_{ij} \times \left[\underbrace{\overline{c'_i c'_j}}_a \times \underbrace{(\overline{c_i} + \overline{c_j})}_b + \underbrace{\overline{c_i} \times c_j'^2}_c + \underbrace{\overline{c_j} \times c_i'^2}_d + \underbrace{c'_i c'_j c'_j}_e + \underbrace{c'_i c'_j c'_i}_f \right] \quad (18)$$

965 Note that the covariance in Eq. (1) is given in the first term of Eq. (18), and, therefore a
 966 diagnostic relation for $\overline{c'_i c'_j}$ (outgoing from the balance of the covariance) can be formulated
 967 based on R_{ij} .

968

969 Dlugi et al. (2014) solved Eq. (18) for $\overline{c'_i c'_j}$ and combined this formula with Eq. (17). This
 970 results in Eq. (20), if for $\overline{c_i} \approx 1 \text{ ppb}$ (ISO) and $\overline{c_j} \approx 10^{-4} \text{ ppb}$ (OH), also the relation $\overline{c_i} \gg \overline{c_j}$ is
 971 considered with

$$972 \quad C_{ij} = \underbrace{\overline{c_i} \times c_j'^2}_b + \underbrace{c'_i c'_i c'_j}_d + \underbrace{c'_i c'_j c'_j}_e \quad (19)$$

$$973 \quad -\overline{c'_i c'_j} = \frac{1}{k_{ij} \cdot \overline{c_i}} \times (RES + k_{ij} \times C_{ij}) - \frac{\overline{c_j}}{\overline{c_i}} \times \overline{c_i'^2} = RE + \frac{C_{ij}}{\overline{c_i}} - \frac{\overline{c_j}}{\overline{c_i}} \times \overline{c_i'^2} \quad (20)$$

974 The same *order of magnitude estimation* as performed for the balances of the variance and
 975 the flux shows that only the second term (d) in C_{ij} (Eq. (19)) contributes to the covariance
 976 (Dlugi et al., 2014). Finally if Eq. (20) is divided by $\overline{c_i} \times \overline{c_j}$ a diagnostic equation for I_s (see Eq.
 977 (1)) is obtained:

$$978 \quad -I_s = \underbrace{\frac{RES}{k_{ij} \times \overline{c_i} \times (\overline{c_i} \times \overline{c_j})}}_I + \underbrace{\frac{\overline{c'_i c'_i c'_j}}{\overline{c_i} \times (\overline{c_i} \times \overline{c_j})}}_{II} - \frac{\overline{c_i'^2}}{\overline{c_i^2}} = RE_{is} + CH_{is} - nvar(ISO)_{is} \quad (21)$$

979 Here only the numerator of the first term (I) in Eq. (21) is unknown, if measurements at one
 980 height could be performed to study segregation as it was done during ECHO 2003 and ATTO
 981 2015. As described by Dlugi et al. (2014) (their Table 3) most terms composing RES can be
 982 estimated by their order of magnitude for ECHO 2003. All other terms can be directly
 983 calculated from measurements. Note that both terms, CH_{is} and the normalized variance of
 984 isoprene $nvar(ISO)_{is}$, originate from R_{ij} (Eq. (18)). The (normalized) variance of isoprene
 985 was shown to correlate well with I_s by experimental data analysis (Dlugi et al., 2014) and



1986 modelling studies (e.g., Patton et al., 2001; Vinuesa and Vilà-Guerau de Arellano, 2005;
1987 Ouwersloot et al., 2011) and was therefore separated from all other terms of the chemical
1988 term that are contained in CH_{is} . This is because the OH mixing ratios and variances are
1989 small compared to the isoprene mixing ratios and variances. The same analysis as for ECHO
1990 2003 was applied to ATTO 2015 data.

1991

1992 At first we compare terms of Eq. (18) for ATTO 2015. The calculation of all terms ($a - e$) of
1993 R_{ij} (Eq. (18)) shows that terms a and c are dominant (Fig. 3) for ATTO 2015 as well as for
1994 ECHO 2003 (see Fig. 12 in Dlugi et al. (2014)). Term a serves to formulate the left side of
1995 Eq. (20). Term c originates from the third term on the right side of Eq. (18), and, finally
1996 becomes $nvar(ISO)_{is}$ in Eq. (21).

1997

1998 Although term c is positive definite, other terms like term a or d in Eq. (18) are not. Therefore
1999 R_{ij} also becomes negative (Fig. 3). The relation between term c of R_{ij} and R_{ij} itself for both
1000 experiments is expressed by the presentation in Fig. 4. The error bars in Fig. 6 and Fig. 7 for
1001 ECHO 2003 are given by the uncertainties of the covariance in I_s (Eq. 1) and R_{ij} as well as
1002 higher moments in σ_i^2 and CH_{is} , if the time delay between time series of ISO and OH is
1003 varied by up to ± 0.2 s. This time shift estimates the influence of wind vector variation inside
1004 the sampling volume, as discussed by Dlugi et al (2014).

1005

1006

1007

1008

1009

1010

1011

1012

1013

1014

1015

1016

1017

1018

1019

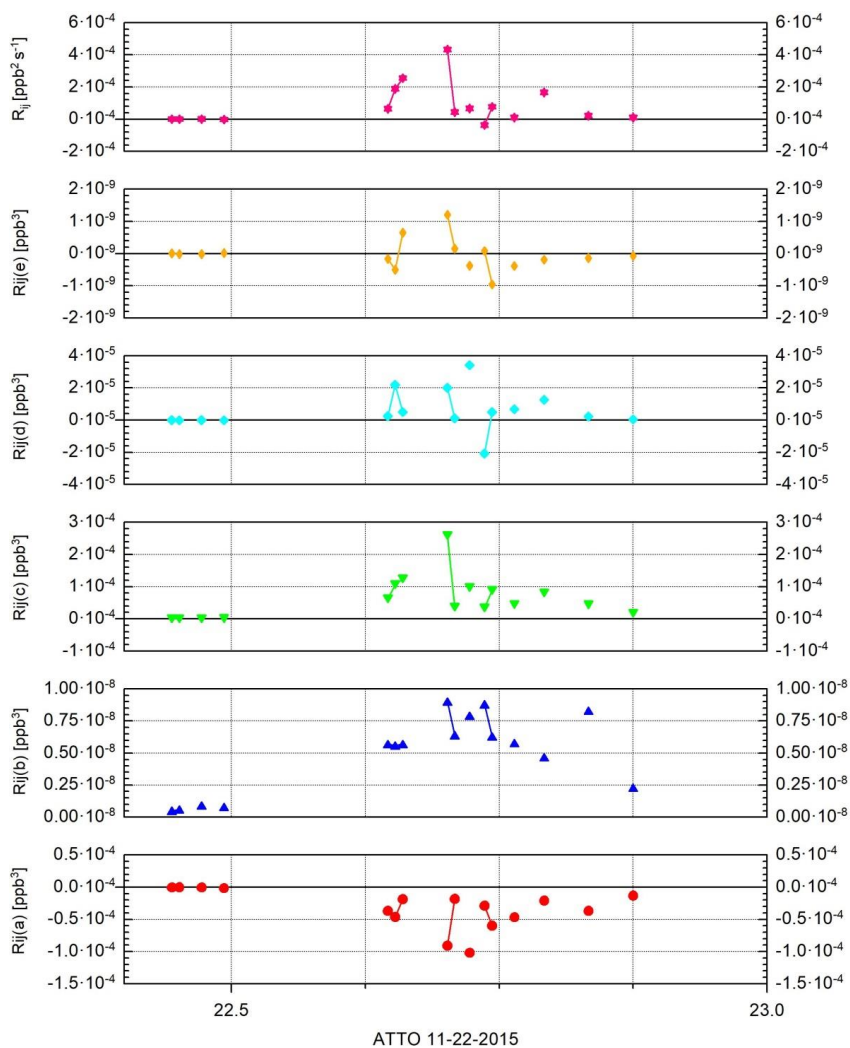
1020

1021

1022

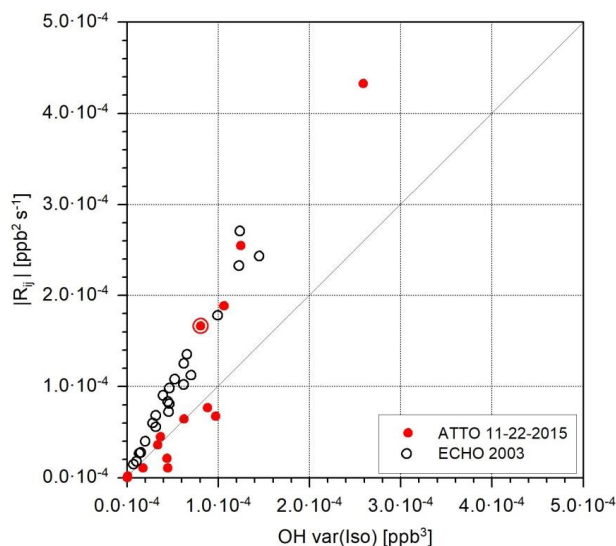


1023
1024
1025
1026
1027



1028

1029 **Fig. 3** The five terms of (Eq. (18)) and R_{ij} for ATTO on 22 November 2015.



1030

1031 **Fig. 4** The magnitude of R_{ij} as function of term c in Eq. (18) for ECHO (25 July 2003) and ATTO (22
 1032 November 2015). Data points before noon are clumped together near zero. (The circle gives
 1033 the data point which deviates from the fit as described in the text).

1034

1035 The importance of the turbulent fluctuations of the isoprene mixing ratio for the magnitude of
 1036 I_s , as pointed out by Patton et al. (2001) and Ouwersloot et al. (2011) from their modelling
 1037 studies, is also proven by these experimental findings, as the reaction term can be well
 1038 described by $(OH \times var(ISO))$ (Fig. 4). For $|R_{ij}| \leq 10^{-4} ppb^2 s^{-1}$ the ECHO 2003 data are
 1039 given by $|R_{ij}| \approx 2.15 (OH \times var(ISO)) \approx k_{ij} (OH \times var(ISO))$, while the ATTO 2015 data
 1040 follow $|R_{ij}| \approx 0.74 (OH \times var(ISO))$ with the exception of one data point (circled, Fig. 4). The
 1041 deviation of the ATTO results from those for ECHO is unknown up to now.

1042

1043 The time behavior of all terms in Eq. (21) for the situation during 22 November 2015 at the
 1044 ATTO tower is given in Fig. 5. For comparison, the same four terms for the ECHO 2003 case
 1045 study are shown in Fig. 6 as given originally by Dlugi et al. (2014).

1046

1047

1048

1049

1050

1051

1052

1053

1054



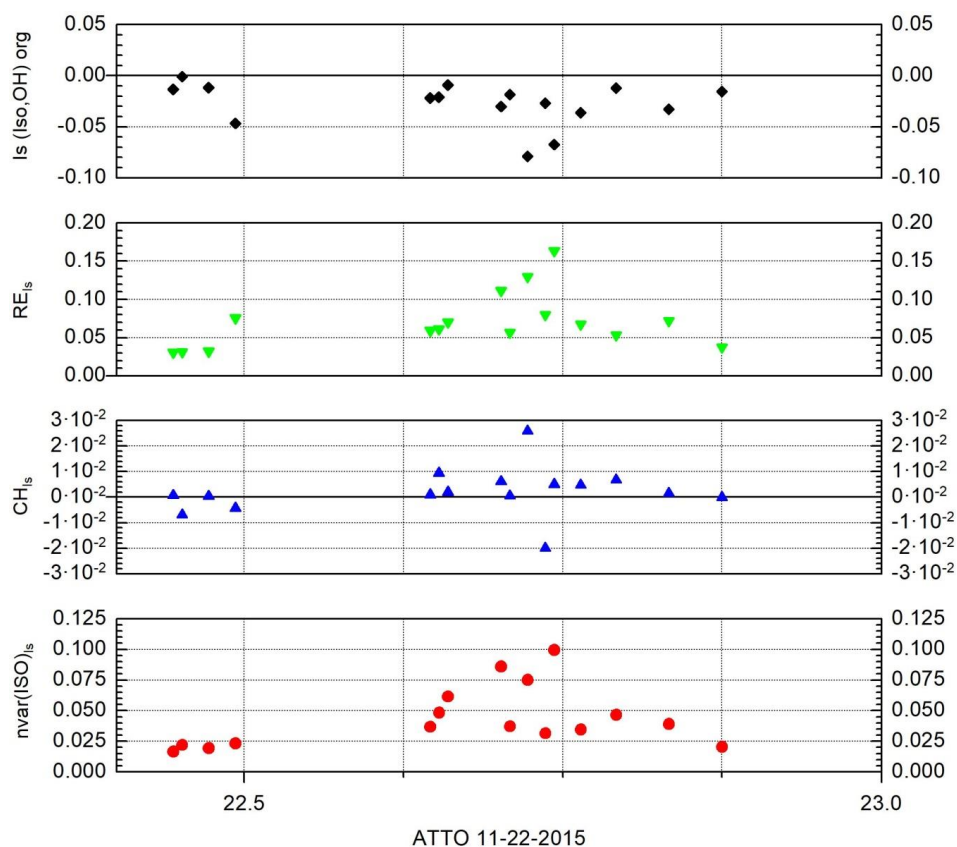
1055

1056

1057

1058

1059



1060

1061

1062

1063

1064

1065

1066

1067

1068

1069

1070

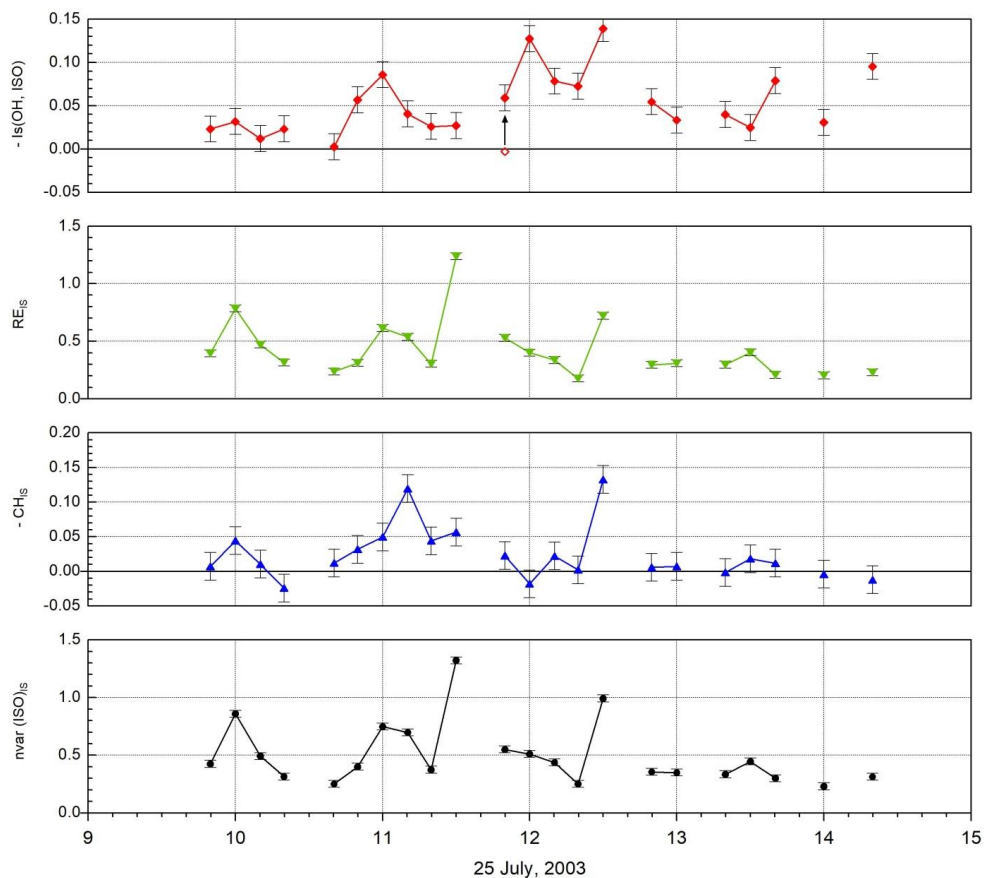
Fig. 5 The four terms of Eq. (21) for ATTO on 22 November, 2015 as function of time. (Note that the calculations of the third moments in Eq. (18) – Eq. (21) are performed in a way that only third order terms are selected which are above 2σ of the minimum value found in the data set.)



1071

1072

1073

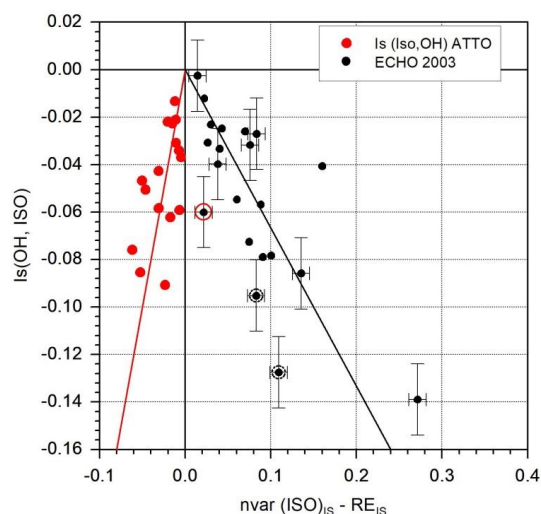


1074

1075

1076

Fig. 6 The four terms of Eq. (21) for ECHO on 25 July, 2003 as function of time (adapted from the original presentation in Dlugi et al. 2014).



1077

1078

Fig. 7 The segregation intensity I_s as function of the difference $nvar(ISO)_{is} - RE_{is}$ according Eq. (21) for the ECHO and the ATTO cases. (Note that the calculations of the third moments in Eq. (18) – Eq. (21) are performed in a way that only third order terms are selected which are above 2σ of the minimum value found in the data set.) The circles around some ECHO 2003 data are explained in the text.

1079

1080

1081

1082

1083

1084 Although the magnitudes of $nvar(ISO)_{is}$, and therefore RE_{is} - but also CH_{is} - differ between
 1085 the two studies by about an order of magnitude (Fig. 5, 6), the segregation intensities, I_s ,
 1086 some meters above the canopy top are comparable in magnitude with $|I_{s,ATTO}| \leq |I_{s,ECHO}|$. In
 1087 both studies, CH_{is} is significantly smaller than $nvar(ISO)_{is}$ and RE_{is} , which are both of
 1088 comparable magnitude. Therefore, $I_s \sim (nvar(ISO)_{is} - RE_{is})$ in Fig. 7. The three marked
 1089 points (Fig. 7) for the ECHO 2003 case belong to two periods of convective conditions
 1090 (black circles) and one case where a correction was applied based on the analysis of the
 1091 ogive for $\overline{c'_i c'_j}$ (red circle) as discussed in more detail by Dlugi et al. (2014) in their sections
 1092 5.3.4 and 4.2.4.

1093

1094 RE_{is} is the residuum determined by the other three terms in Eq. (21). None of these terms is
 1095 near zero for ECHO 2003 (Fig. 6) as well as ATTO 2015 (Fig. 5). We find $nvar(ISO)_{is} > RE_{is}$
 1096 for ECHO 2003 which proves $CH_{is} \neq 0$ with an average value of $nvar(ISO)_{is} \approx 0.42$. For
 1097 $I_s = -0.16$ (extrapolated from the ECHO 2003 data in Fig. 7) one obtains a mean value for
 1098 $nvar(ISO)_{is} - RE_{is} = 0.24$, which results in mean values for $RE_{is} \approx 0.18$ and $CH_{is} \approx 0.08$
 1099 according to Eq. (21) for the ECHO 2003 case. But some data points for ECHO 2003 in Fig.
 1100 7 (circles around data points) fulfill the conditions $nvar(ISO)_{is} - RE_{is} < I_s$, which requires not
 1101 only $CH_{is} < 0$ but even $|nvar(ISO)_{is}| < |RE_{is}|$ as discussed by Dlugi et al. (2014). The term
 1102 CH_{is} - e.g., the triple moment in term (d) (Eq. (19)) - is either negative or positive (Fig. 5, 6).

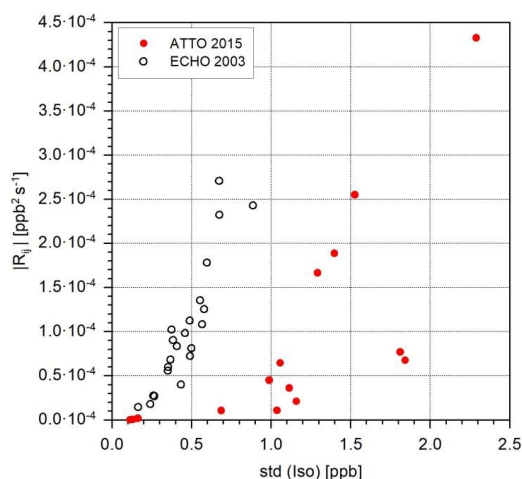


1103 For this ATTO case the term RE_{is} is always larger than $nvar(ISO)_{is}$. I_s is therefore dominated
 1104 by this residual term (Fig. 5, 6) which describes the interactions between the turbulent flow
 1105 field with the fields of both scalars.

1106

1107 Note that R_{ij} (eq. (18); Fig. 8) increases with increasing variance of the reactants. As mixing
 1108 ratios and variances of isoprene are much larger than those of OH , the standard deviation of
 1109 isoprene ($\sigma_i = \overline{(c_i'^2)}^{1/2} = std(ISO)$) is a main driver in the chemical terms, and, therefore,
 1110 also for I_s (Eq. (3)) with a correlation coefficient $R = 0.91$ for ECHO 2003 and $R = 0.79$ for
 1111 ATTO 2015 (Fig. 8). This reflects the important influence of this term c of Eq. (18) and of σ_i in
 1112 Eq. (3) (Fig. 8). But the influences of turbulent transport and mixing in term RES respectively
 1113 RE_{is} may even exceed the magnitude of $nvar(ISO)_{is}$ (Fig. 7). I_s , therefore, becomes
 1114 controlled by chemical as well as dynamic and mixing processes enhancing the variances of
 1115 the reactants, respectively σ_i (and / or σ_j). In addition the variation of the surface source
 1116 strength E_{oi} in space and time influences σ_i .

1117



1118

1119 **Fig. 8** R_{ij} (see Eq. (18)) as function of the isoprene standard deviation for ECHO 2003 and ATTO
 1120 2015.

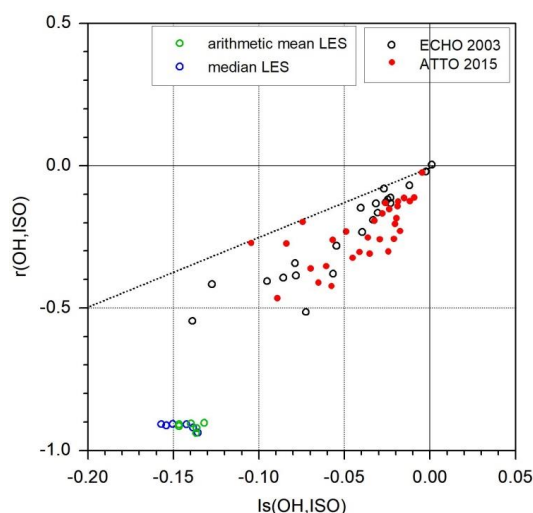
1121

1122 The quantities σ_i , σ_j and the correlation coefficient r_{ij} from the numerator in Eq. (3) define the
 1123 magnitude of I_s . The correlation coefficient $r_{ij} = r(OH, ISO)$ from the field increases for both
 1124 cases non-linearly with increasing I_s (Fig. 9). All values of r_{ij} from experiments are found
 1125 below a line $|r_{ij}| = 2.5 \cdot |I_s|$ (for $-0.4 \leq I_s \leq 0$) and are smaller than $r_{ij} = -0.6$. Note that this
 1126 relation is very similar for ATTO 2015 and ECHO 2003 (Fig. 9).

1127



1128 Dlugi et al. (2010; 2014) discussed the influence of instrumental (white) noise on r_{ij} . The
1129 contribution of noise to the isoprene mixing ratio is small (e.g., Spirig et al., 2005) and only
1130 influences σ_i by less than 5% for ECHO 2003 and by less than 1% for ATTO 2015. In
1131 contrast, the signal to noise ratio of the measured mixing ratios of the hydroxyl radical is
1132 sometimes only 3.
1133



1134

1135 **Fig. 9** The correlation coefficient in Eq. (3) between **OH** and isoprene for ECHO 2003 and ATTO
1136 2015 and from the LES model for a layer of 10 m to 30 m above the surface (Ouwensloot et
1137 al., 2011).

1138

1139 The σ_j is influenced in such case by the impact of noise on the variance and becomes larger
1140 by up to 15%. Therefore, if the standard deviation σ_j increases by up to 15%, r_{ij} in Eq. (3)
1141 becomes smaller by this magnitude as compensation. If this estimate is applied to all data in
1142 Fig. 9, the largest correlation coefficient from ECHO 2003 would be about $r_{ij} = -0.65$. This
1143 is still below the theoretically applied $r_{ij} \geq -0.7$ for modelling studies (e.g., Table 3).
1144 Ouwensloot et al. (2011) calculated r_{ij} explicitly in their LES model and obtained medians
1145 and arithmetic means of about $r_{ij} \approx -0.9$ (Fig. 9) for the lowest layers between 10 m and 30
1146 m above the surface. A significant difference exists between the correlation coefficients from
1147 field measurements and modelling. On the other hand the covariances (in Eq. (2)) and I_s (in
1148 Eq. (1)) are rarely modified by instrumental noise as shown for the background signals of the
1149 PTR-MS instrument and the LIF for the ECHO 2003 study. This means that these signals
1150 have characteristics near white noise and, therefore, are not correlated (e.g., Wu et al., 2007;
1151 Sachs and Hedderich, 2006).

1152



1153 4. Variability of Segregation Intensity

1154

1155 4.1. Relation between Segregation Intensity and Surface Flux

1156

1157 In addition to the results discussed by Dlugi et al. (2010, 2014), the segregation intensity can
1158 be presented in terms of Eq. (6) to establish an empirical relationship to the turbulent flux of
1159 isoprene. As mentioned before, such a direct proportionality between I_s and $\overline{w'c'_i}$, is stated by
1160 Kaser et al. (2015) and others. In Section 3 (3.3; 3.4) we discussed which prognostic and
1161 diagnostic relations exist to establish such a relation.

1162

1163 The analysis of the data from ECHO 2003 and ATTO 2015 related to Eq. (6) yields the
1164 results given in Fig. 10 for all isoprene fluxes. During ECHO 2003, the influence of
1165 convective transport by clouds was occasionally observed and caused significant up- and
1166 downdrafts at the main tower only 7 m above canopy top (Dlugi et al., 2014). The downward
1167 motion was observed also for sensible and latent heat and resulted in situations with net
1168 downward transport of isoprene (note that a covariance $\overline{w'\alpha'}$ is always composed of positive
1169 (upward) and negative (downward) values of vertical wind velocity w and the corresponding
1170 values of α during the averaging time T). The downward (negative values of w) motion was
1171 observed to dominate in the range below $10^{-2} Hz$ for some averaging periods $T = 600 s$. This
1172 caused the cumulative (flux) covariance (the *ogives*) to be negative in this frequency range.
1173 For higher frequencies the ogives were positive, which can be related to the influence of the
1174 emission flux. Thus $\overline{w'c'_i} = 0$ (see Fig. 10) results from spectral compensation of upward and
1175 downward motion (see also Fig. 12 in Dlugi et al. 2014 and the discussion on Fig. 7).

1176

1177 If only the upward-directed (positive) turbulent isoprene flux values from measurements near
1178 canopy top are considered (Fig. 11), the statistical correlation with I_s improves. Compared to
1179 the complete results in Fig. 10 for ECHO 2003, the coefficient of determination, Eta_{adj}^2 ,
1180 increases from $Eta_{adj}^2 \approx 0.40$ to $Eta_{adj}^2 \approx 0.56$, also together with the correlation coefficient.
1181 But still about 44% of the variance is not accounted for by the linear regression in Fig. 11
1182 (e.g., Sachs and Hedderich, 2006). This result cannot be improved even if the other terms in
1183 Eq. (6) would perfectly correlate ($R = 1; Eta_{adj}^2 = 1$) with I_s . A comparable result is obtained
1184 for on 22 November during ATTO 2015.

1185

1186 A negative correlation between I_s and the measured isoprene flux is given in Fig. 10 or Fig.
1187 11 and is also described by Kaser et al. (2015), but with $Eta_{adj}^2 = 0.1156$ and a correlation
1188 coefficient $|R| = 0.34$. Therefore, less than 12% of the variance of these data from a flight



1189 track in the ABL for the relation between I_s and $\overline{w'c'_i}$ is described by this regression (see Fig.
1190 S5 in Kaser et al., 2015).

1191

1192 The ECHO 2003 and ATTO 2015 measurements were performed near the canopy top
1193 ($z/z_i \cong 0.03$) (see: Section 2.), while the NOMADSS 2013 results are calculated from aircraft
1194 measurements at $z/z_i \approx 0.4$ with $z_i =$ ABL height. We applied the convective boundary layer
1195 (CBL) scaling for fluxes (e.g., Moeng and Wyngaard, 1984; Wyngaard and Brost, 1985;
1196 Moeng and Sullivan, 1994; Hess, 1992; Patton et al., 2003) to a measured mean for the
1197 isoprene flux of about 0.1 ppb m s^{-1} for this flight track (see Fig. S5 (supplement), Kaser et
1198 al., 2015) and estimated a surface flux in the range of $1 - 1.3 \text{ ppb m s}^{-1}$. This result agrees
1199 to average isoprene fluxes given by Su et al. (2015) (in their Fig. S5) determined in the same
1200 region for conditions around noon in June 2013.

1201

1202 To understand both findings we compare them with the results of the first studies on
1203 balances of second moments of scalars and their relation to the mean fields of related
1204 quantities in the ABL as presented by Stull (1988) based on research done by Lenschow et
1205 al. (1980), André et al. (1978), Deardorff (1974), Caughey and Palmer (1979) and Zhou et al.
1206 (1985) for virtual potential temperature θ_v and by Deardorff (1974) and Lenschow et al.
1207 (1980) for specific humidity q . These authors performed their analysis on data of day 33 of
1208 the Wangara – experiment 1967. Further references to analysis of this kind are summarized
1209 and discussed - for example - in Haugen (1973), Sorbjan (1989) or Garrett (1992).

1210

1211 The analysis of the balances of variances ($\overline{\theta_v'^2}$ or $\overline{q'^2}$) show that the gradient *production term*
1212 GP_{var} (see Eq. (11)) has maximum values at the surface. The magnitude of GP_{var} decreases
1213 with increasing height with minima around $z/z_i \approx 0.2$ for $\overline{q'^2}$ and in the interval $0.5 \leq$
1214 $z/z_i \leq 0.8$ for $\overline{\theta_v'^2}$ during the early afternoon. As the contribution of the production term GP_{var}
1215 decreases with increasing height, the contributions of other terms in the budget increases.
1216 Therefore, a relation between term GP_{var} respectively the turbulent flux $\overline{w'c'_i}$ in Eq. (11a) and
1217 $\overline{c_i'^2}$ is only established near the Earth surface where a certain correlation exists, but with a
1218 correlation coefficient $|R| < 0.77$ between I_s and $\overline{w'c'_i}$ (Fig. 10, Fig. 11).

1219

1220

1221

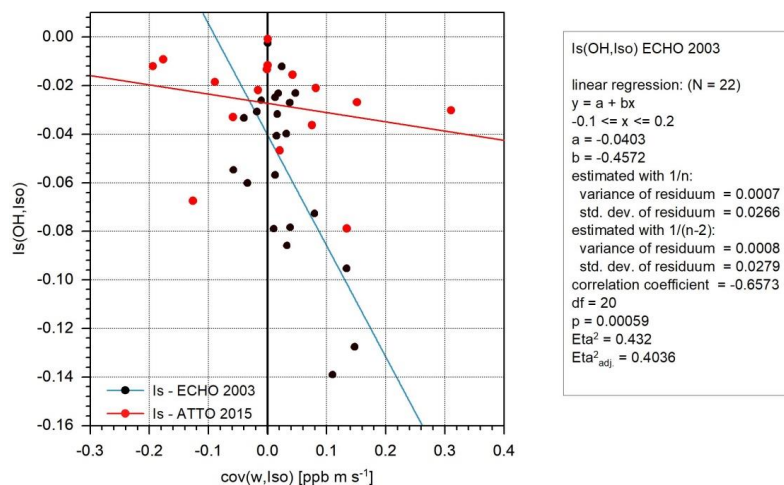
1222

1223

1224



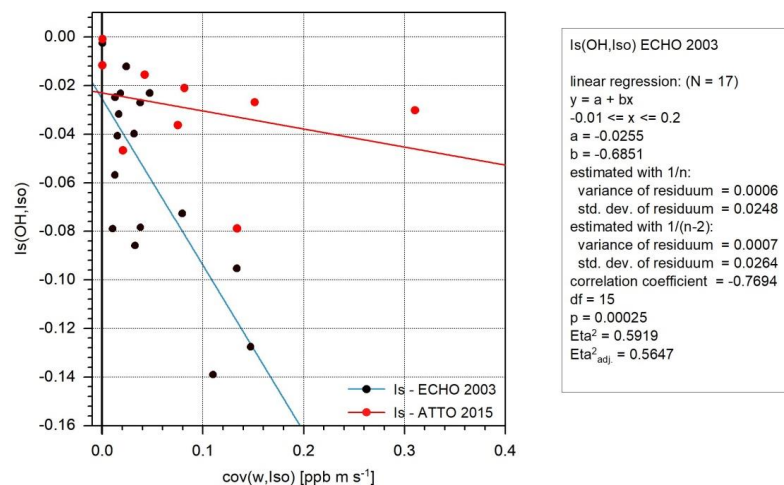
1225



1226

1227 **Fig. 10** The segregation intensity, I_s , (ECHO: 25 July, 2003 and ATTO: 22 November, 2015) as
 1228 function of the turbulent isoprene flux above canopy top with the influence of net downward
 1229 and upward motion. (Linear regression for ATTO 2015: $N = 16$; $a = -0.0273$; $b = -0.038$;
 1230 correlation coefficient = -0.2297)
 1231

1232



1233

1234 **Fig. 11** The segregation intensity, I_s , (ECHO: 25 July, 2003 and ATTO: 22 November, 2015) as
 1235 function of only the upward directed turbulent fluxes of isoprene. (Linear regression for ATTO
 1236 2015: $N = 9$; $a = -0.023$; $b = -0.0742$; correlation coefficient = -0.3196)
 1237

1238

1239



1240 With increasing height in the ABL, $\overline{c_i'^2}$ (respectively $\sigma_i = (\overline{c_i'^2})^{1/2}$) is also determined by the
1241 growing influence of other terms (and even vertical advection), so that the correlation
1242 between I_s and the flux $\overline{w'c_i'}$ in GP_{var} decreases significantly. This agrees with the result
1243 obtained by Kaser et al. (2015) which becomes different for fluxes measured near the top of
1244 a forest (Fig. 10 and Fig. 11) in ECHO 2003 or ATTO 2015. As discussed in Section 3.4 the
1245 near surface isoprene flux (Eq. (14)) is not primarily determined by the convective (heat) flux
1246 but by the production term (i) in Eq. (12) and by the chemical reaction term R_{wi} (Eq. (13),
1247 Fig. 2).

1248

1249 Although our CBL scaling - applied to the fluxes given for NOMADSS for the flight level at
1250 $z/z_i \approx 0.4$ down to the surface - yields reliable results, the fluxes of isoprene and sensible
1251 heat given by Kaser et al. (2015) at $z/z_i \approx 0.4$ are not significantly correlated to each other.
1252 Note that even in the NOMADSS 2013 case (flight RF13), where free convective conditions
1253 in the ABL around noon may exist (e.g., Su et al., 2015), the correlation between the fluxes
1254 of sensible heat and isoprene ($Eta_{adj}^2 = 0.1781$) at the mean flight level $z/z_i \approx 0.4$ is weak
1255 (Fig. S6 in Kaser et al., 2015), as 82% of the variance is not explained by the correlation
1256 (e.g., Sachs and Hedderich, 2006).

1257

1258 The NOMADSS sensible heat flux data show dominant up- and downdrafts – as it should be
1259 observed in a CBL – with most results in a range $-0.03 < \overline{w'T'} < 0.13 K m s^{-1}$. Note that
1260 some larger positive and negative fluxes are “*excluded from fit*” (Fig. S6 in Kaser et al.,
1261 2015). If we applied the convective scaling also to estimate the mean sensible heat flux at
1262 the surface, values around $H_s \approx 0.1 K m s^{-1}$ are obtained, again also in agreement with
1263 results reported by Su et al. (2015).

1264

1265 In addition, other observations in the CBL show that at $z/z_i \approx 0.4$ the amount of downward
1266 (negative) fluxes are between 10% to 40% (e.g., Stull, 1988; Patton et al., 2003). Su et al.
1267 (2015) assume a relation for heat transport between entrainment flux and surface flux of 20%
1268 as a mean value for the CBL. If a higher correlation exists between both fluxes at the
1269 surface, this relation is reduced by downdrafts of sensible heat with increasing height in the
1270 CBL. Therefore a correlation between I_s and $\overline{w'c_i'}$, as found near the surface, vanishes with
1271 increasing height in the ABL, consistent with other experimental findings and results from
1272 modelling.

1273

1274

1275



1276 **4.2. Is there an Upper Limit for the Segregation Intensity in the OH – Isoprene**
1277 **Reaction?**

1278

1279 **4.2.1 The Relation between Covariance and Product of the Means**

1280

1281 Most results on segregation for atmospheric conditions are derived from modelling. A
1282 selection of such results for reaction Eq. (4) and a comparison with experimental findings is
1283 given in Table 3. Maximum values for I_s near the Earth surface, respectively near canopy top
1284 ($z_R \approx h_c$ and $z_R/z_i < 0.05$), are in the range $-0.27 \leq I_s \leq -0.02$, if results from experiments
1285 and LES models are considered.

1286

1287 Kaser et al. (2015) report on a range of I_s from flight RF13 of $-0.17 \leq I_s \leq -0.09$ and for
1288 flight RF17 of $-0.19 \leq I_s \leq -0.085$ at a mean flight level z_F of about $z_F/z_i \approx 0.4$. They
1289 mention that “during flight R17, local segregation was measured as large as -0.3 ” and they
1290 relate the high values to “surface heterogeneity larger than typical PBL scales”, e.g., to
1291 source areas of this size with higher isoprene emission fluxes.

1292

1293 Note that with their time resolution for OH measurements of 30 s ($0.03\bar{3}\text{ Hz}$) and the mean
1294 flight velocity of 100 m s^{-1} they obtained one OH data point every 3 km , 17 data points for a
1295 51 km flight leg and 34 data points for a 102 km leg. The spectral maximum of I_s is given for
1296 a time scale of about 730 s , which includes about 24 data points and corresponds to a root
1297 mean square of about 20%.

1298

1299 The surface heterogeneities in the emission rates, where high values in the order of $I_s \approx$
1300 -0.3 were determined by Kaser et al. (2015), are related to surface scales larger than z_i . For
1301 the flight RF13 and $z_i \approx 2200\text{ m}$, spatial scales of the order of three to six times the value of
1302 z_i may cause such high values. But for such a flight leg of about 6.6 km to 13.2 km only about
1303 two to four (or five) data points from the OH instrument are available for the calculation of I_s ,
1304 which results in a root mean square larger than 47%.

1305

1306 For comparison, the time resolution for the analysis of the data of OH and isoprene during
1307 ECHO 2003 and ATTO 2015 was 0.2 Hz and 0.067 Hz , respectively, leading to 120 OH data
1308 points (respectively 40 data points) in the time intervals of 600 s , which were considered for
1309 the analysis by Dlugi et al. (2010) and Dlugi et al. (2014), respectively, and in this study for
1310 ATTO 2015. The root mean square error of these data sets is about 9.1% and 15.8%,
1311 respectively.

1312



1313 To introduce a higher time resolution, Kaser et al. (2015) extended the OH - spectra from
1314 about 0.03 Hz to higher frequencies using spectra of O_3 - variance and covariance, $\overline{O_3'ISO'}$,
1315 as a surrogate of $\overline{OH'ISO'}$. This approach is not justified a priori, because the mixing ratios of
1316 OH and O_3 are not related to each other in a 1:1 relation.

1317

1318 Based on this modified data set, they present a wavelet analysis for the cross spectrum of
1319 the covariance $\overline{c_i'c_j'}$ for the wavelet scale $> 80\text{ s}$ to show that I_s maxima occur at time scales
1320 between 500 s to 1000 s . These time scales correspond to spatial scales of about 50 km and
1321 100 km , according to the mean flight velocity of 100 m s^{-1} .

1322

1323 Therefore, their statement, that “an increase in isoprene flux” – by such a strong surface
1324 source – “should lead to an enhanced production of I_s as observed in the real data sets”
1325 (Kaser et al., 2015), is not based on conclusive results, as also described in Section 4.1. As
1326 discussed above, this result is not surprising, because the statement supposes that the
1327 emission flux, E_{i0} , is directly related to $\overline{w'c_i'}$ at any height in the ABL and – in addition – that
1328 this isoprene flux significantly correlates with I_s . But this relation, $I_s \approx f(\overline{w'c_i'})$, can only exist
1329 near the surface if the variance (and therefore σ_i) is mainly controlled by the term GP_{var} in
1330 Eq. (9) and Eq. (11). At the flight level of $z_F/z_i \approx 0.4$, the low correlation found by Kaser et al.
1331 (2015) proves that this relation is no longer valid and other terms in the balance of the
1332 variance are of larger influence as described for heat and moisture from the analysis of
1333 earlier studies in Stull (1988).

1334

1335 Kaser et al. (2015) also suggest that the covariance $\overline{c_i'c_j'}$ in Eq. (1) is directly proportional to
1336 the product of mean mixing ratios, $\overline{c_i} \times \overline{c_j}$. The only data set showing such a relationship was
1337 presented by Dlugi et al. (2014) and is given in Fig. 12 together with an extended analysis of
1338 ECHO 2003, data from ATTO 2015, and the values modelled by LES for the lowest layer and
1339 inhomogeneous conditions (Ouwensloot et al., 2011). In addition, two data points from flight
1340 RF13 and RF17 are added from Kaser et al. (2015), which are estimated from their Table 1
1341 and Table S2 (in their supplement). For RF13 and RF17, only the mean mixing ratio of the
1342 PTR-MS instrument measuring isoprene is used as reported in their Table S2. Therefore only
1343 mean values of the covariances can be calculated, but not their ranges as given for I_s in
1344 Table 3 (according to Table 1 of Kaser et al., 2015).

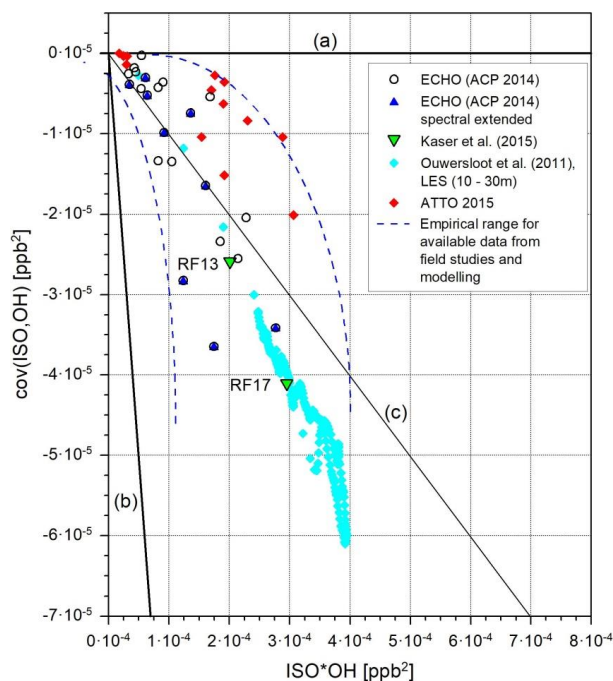
1345



1346
1347
1348
1349
1350
1351
1352
1353
1354
1355
1356
1357
1358
1359
1360
1361
1362
1363
1364
1365
1366
1367
1368
1369

Tab. 3 Overview of different terms of Eq. (1) from modelling (1 – 6) and experiments (7 - 9) for the reaction $ISO + OH$ (Sk = skewness; ν = frequency; c_i = mixing ratio; h_c = canopy height; z_i = ABL – height; u_* = friction velocity)

Authors	I_s	Da_c	$r_{ISO,OH}$	Spectral Range	Comments
1 Peterson and Hottel (1999)	-0.27 (LES) -0.4 (1-D)	≈ 0.65	n.a.	n.a.	their Tab 2.6 and Chpt. 5 for: $z/z_c < 0.05$
2 Patton et al. (2001)	-0.175 (near h_c) (LES)	0.17	≥ -0.7	$4 \cdot 10^{-4} \leq \nu \leq 0.16 \text{ Hz}$	$Sk_{iso} \ll$ measured $Sk_{iso,c}$ therefore r_{ij} (model) $>$ r_{ij} (experiment)
3 Verver et al. (2000)	below -0.1 below -0.02	≈ 0.18 ≈ 0.05	n.a.	n.a.	Morning hours and afternoon Diurnal cycle of Da_c and I_s
4 Vinuesa and Vilà-Guerau de Arellano (2005)	-0.17 -0.1 (LES)	≈ 0.6 ≈ 0.3 (LES)	≥ -0.75	n.a.	near $z/z_c \approx 0.1$ near $z/z_c \approx 0.05$
5 Ouwersloot et al. (2011)	-0.195 (max) (LES) -0.07 to -0.09 (LES)	about 0.2	> -0.7		Inhomogeneous isoprene emission; for homogeneous isoprene emission: r_{ij} increases with increasing R_{ij} (Eq.(1))
6 Kaser et al. (2015)	LES: -0.3 / -0.47 (a) -0.1 to -0.3 (b)	about 0.4	≥ -0.7 (see (2.))	about $4 \cdot 10^{-4} \leq \nu \leq 0.1 \text{ Hz}$	(a) $z/z_c \approx 0.027$ near $z = h_c$ homogeneous / inhomogeneous emission (b) $z/z_c \approx 0.4$; homogeneous / inhomogeneous emission
7 Kaser et al. (2015)	-0.13; -0.09 to -0.17 -0.14; -0.085 to -0.195 max: -0.19 to -0.3	≈ 0.42 n.a.	estimate < -0.7	$4.5 \cdot 10^{-4} \leq \nu \leq 0.03 \text{ Hz}$ $8 \cdot 10^{-4} < \nu < 2 \cdot 10^{-3} \text{ Hz}$	mean and variation for flight track; variation for high ISO sources
This work: Based on data from Dlugi et al. (2010, 2014) from ECHO	-0.15 to -0.01 -0.21 to -0.02*	$0.01 < Da_{h_c} < 0.1$ $0.03 < Da_{h_s} < 0.3$	< -0.56 ≤ -0.65	$1.6 \cdot 10^{-3} \leq \nu \leq 0.2 \text{ Hz}$ $5 \cdot 10^{-4} \leq \nu \leq 0.2 \text{ Hz}^*$	$\tau_{r1} = h_c / u_*$ (see 2.); $z/z_c \approx 0.03$; *spectral contributions below $1.6 \cdot 10^{-3} \text{ Hz}$ contribute up to 23% to I_s ; τ_{r1} from Lagrangian diffusion with $\tau_{r2} \approx (3.0 \text{ to } 4.0) \tau_{r1}$ (see Chpt. 4.3)
This work: Based on data from ATTO 2015, 22 November	-0.11 to -0.01	$0.04 < Da_{h_s} < 0.1$	< -0.5	$1.6 \cdot 10^{-3} \leq \nu \leq 0.2 \text{ Hz}$	τ_{r2} from Lagrange diffusion (see 8); $z/z_c \approx 0.04$



1370

1371

Fig. 12 The covariance between isoprene (*ISO*) and *OH* as function of the product of their mean values according to Eq. (1). Line a): $I_s = 0$; line b): $I_s = -1.0$; line c): $I_s = -0.1$. The data from Kaser et al. (2015) are for their measurements with PTR-MS (their Tables 1 and S2). The LES Data are from Ouwersloot et al. (2011) for the lowest layers between 10m – 30m above ground and the inhomogeneous case. The spectral extended analysis for ECHO 2003 is described in the text.

1372

1373

1374

1375

1376

1377

1378

1379

For ECHO 2003, the spectral analysis was extended to time intervals $\Delta T = 1800$ s to cover a range of lower frequencies of up to $5.6 \cdot 10^{-4}$ Hz (which includes larger spatial scales, if the Taylor hypothesis is applied) compared to the results for the frequency interval

1380

$1.7 \cdot 10^{-3}$ Hz $\leq \nu \leq 0.2$ Hz, as originally given by Dlugi et al. (2014) in their Fig. 8. By

1381

increasing the time interval, the number of values for the covariance in Fig. 12 is smaller than

1382

for the original ECHO results for $\Delta T = 600$ s (Dlugi et al., 2014; Fig. 8). Note that the spectral

1383

range given for $I_s(\nu)$ by Kaser et al. (2015) is for the frequency range of about $4.5 \cdot 10^{-4}$ Hz \leq

1384

$\nu \leq 0.033$ Hz, with an artificial extension to higher frequencies.

1385

1386

1387

1388

Extending the time interval for the ECHO 2003 case I_s becomes larger by about 18% to 27%

1389

as contributions of lower frequencies are added. As discussed by Dlugi et al. (2010), the

1390

analysis for larger time intervals than 600 s was performed in the way that a symmetric linear

1391

Sawitzki-Golay low pass filter signal was subtracted from the time series (Press et al., 1991).



1392 This method is different compared to the analysis for shorter time intervals but also fulfilled
1393 the criterion for stationarity (Beier and Weber, 1992).

1394

1395 In Fig. 12, almost all values of the covariance from ECHO 2003 that are smaller than
1396 $\overline{c'_i c'_j} = -2.1 \cdot 10^{-5} ppb^2$ are above the line c), which is for $I_s = -0.1$. If one numerically fits the
1397 original ECHO results (Dlugi et al. 2010, 2014), a relation, $-cov(ISO, OH) \sim (\overline{ISO} \times \overline{OH})^n$,
1398 $n > 2$ is obtained. The contribution for frequencies below $1.7 \cdot 10^{-3} Hz$ will significantly
1399 enlarge I_s (see also Fig. 13), but does not change such a relation. The result for research
1400 flight RF13 is within this range of data from ECHO 2003. Also the results for RF17 are on the
1401 left side of line c) and even agree to results obtained by the LES modelling study of
1402 Ouwersloot et al. (2011) for the inhomogeneous distribution of emission sources. Here,
1403 results for the lowest layer between 10 m to 30 m above ground are presented. No difference
1404 is observed between modelled and observed data for this relation.

1405

1406 Following this non-linear relation, the segregation intensity becomes independent from the
1407 product of mean mixing ratios with increasing covariance. For example for $cov(ISO, OH) =$
1408 $-7 \cdot 10^{-5} ppb^2$ one estimates by this relation a mean of about $\overline{ISO} \times \overline{OH} \approx 2.5 \cdot 10^{-4} ppb^2$, and
1409 therefore, $I_s \approx -0.28$, a value in the range of the maximum estimated by Butler et al. (2008)
1410 or Kaser et al. (2015). All available data are below $\overline{ISO} \times \overline{OH} = 4 \cdot 10^{-4} ppb^2$ (Fig. 12).

1411

1412 The covariance is given by Eq. (2) and leads to Eq. (3). The normalized standard deviations
1413 $\sigma_i/\overline{c_i} = \sigma_{ISO}/\overline{ISO}$ and $\sigma_j/\overline{c_j} = \sigma_{OH}/\overline{OH}$ approach two bounds, a lower one for increasing
1414 mixing ratios and an upper one near the detection limits (DL) for OH and isoprene (see also
1415 Fig.6 in Dlugi et al., 2014). For example for the ECHO 2003 case and mixing ratios near DL
1416 one obtains $\sigma_{ISO}(DL)/\overline{ISO}(DL) \approx 2.6$ and $\sigma_{OH}(DL)/\overline{OH}(DL) \approx 2.8$. For increasing mixing
1417 ratios $\sigma_{ISO}/\overline{ISO} \approx 0.5$ and $\sigma_{OH}/\overline{OH} \approx 0.25$ are determined. The third term in Eq. (3) is the
1418 correlation coefficient $r_{ij} = r(ISO, OH)$, which increases with increasing product $\overline{ISO} \times \overline{OH}$ (or
1419 I_s in Fig. 9) and approaches zero for $\overline{ISO} \times \overline{OH} \rightarrow 0$ (see Fig. 7 and Fig. 8 in Dlugi et al.,
1420 2014). Therefore, even if the product of normalized standard deviations near DL is of the
1421 order of

1422
$$\sigma_{ISO}(DL)/\overline{ISO}(DL) \times \sigma_{OH}(DL)/\overline{OH}(DL) \approx 2.6 \times 2.8 \approx 7.3 ,$$

1423 the correlation coefficient becomes small, and therefore $|I_s| < 0.07$ for such conditions. For
1424 increasing mixing ratios the correlation coefficient $r(ISO, OH)$ for ECHO 2003 is determined
1425 to be in the range (Table 3)



1426
$$-0.5 \leq r(ISO, OH) \leq -0.6 \leq (-0.65).$$

1427 For these conditions one obtains

1428
$$I_s \approx r_{ISO,OH} \times \frac{\sigma_{ISO} \times \sigma_{OH}}{c_{ISO} \times c_{OH}} \approx -0.6 \times 0.5 \times 0.25 \approx -0.075$$

1429 if high mixing ratios of both reactants exist together. Therefore maxima of I_s exist in between
 1430 these two limits, and obviously values of $-1 \leq I_s \leq -0.35$ are not approached in an
 1431 atmospheric boundary layer for conditions as found during ECHO 2003, ATTO 2015 or
 1432 NOMADSS (Kaser et al., 2015). The above mentioned non-linear relation leads to an
 1433 empirical upper limit of the order of $|I_s| < 0.35$ in the ABL, in agreement also with results from
 1434 modelling (Table 3).

1435

1436

1437

1438 4.2.2 The Relation between Segregation Intensity and Coherent Motion

1439

1440 The transport and mixing processes near canopy top are controlled by non-local coherent
 1441 down- and updraft eddy motion (e.g., Raupach et al., 1991, 1996; Katul et al., 1997; Cava et
 1442 al., 2006). The features of coherent motion can be analyzed by the cumulant expansion
 1443 method (CEM), which couples the imbalance $\Delta S_0 = S_2 - S_4$ in the contributions of *sweeps* S_2
 1444 and *ejections* S_4 to the turbulent flux, $\overline{w'\alpha'}$, of a quantity α ($= u, c_i, T$) to the third mixed and
 1445 non-mixed moments of this (vertically) transported quantity (e.g., Katul et al., 1997). Here S_2
 1446 ($w' < 0, \alpha' > 0$) and S_4 ($w' > 0, \alpha' < 0$) represent the quadrants II and IV of the quadrant
 1447 principle (e.g., Antonia, 1981; Shaw, 1985) with the other two contributions by *outward* (S_1)
 1448 and *inward* (S_3) interactions. In this way a physical turbulent transport of isoprene variance,
 1449 $\overline{w'c'_i c'_i}$, is related to methods and concepts applied to the statistical analysis of time series
 1450 and the probability density functions for w' , α' and $\overline{w'\alpha'}$ (e.g., Nakagawa and Nezu, 1977;
 1451 Raupach, 1981; Katul et al., 1997). The quantity $\overline{w'c'_i c'_i}$ is given in the divergence term
 1452 $TT_{z,var}$ of Eq. (11b) and represents the influence of *ejections* S_4 as a normalized quantity
 1453 $M_{21} = \left(\overline{w'c'_i c'_i} / \sigma_w \sigma_c^2 \right)$ if CEM is applied.

1454

1455 Dlugi et al. (2014) showed that a correlation exists between the two dominant terms of the
 1456 diagnostic equation for I_s (Eq. (21)), $nvar(ISO)_{is}$, and RE_{is} , and M_{21} for the ECHO 2003
 1457 case. The contribution by sweeps – represented by $M_{12} = \left(\overline{w'w'c'_i} / \sigma_w^2 \sigma_c \right)$ – shows only a
 1458 week correlation with $nvar(ISO)_{is}$ and RE_{is} . The same analysis on data from ATTO 2015
 1459 leads to a comparable result. In both experiments *ejections* (S_4), with a time duration D_e ,
 1460 contribute to the flux in each time interval of ten minutes. We found $D_e = 34\%$ (ECHO 2003)



1461 and $D_e = 32\%$ (ATTO 2015) if the contributions of all quadrants are considered. For the
1462 contribution by sweeps (S_2) the time duration D_s is about 48% of the total time in each. In
1463 addition, the percentage contributions of sweeps and ejections to the total flux are
1464 comparable to their time durations and are below 100% for both experiments.

1465

1466 Note that the quantity $\overline{w'c'_i c'_i}$ is not given in the flux balance equation (Eq. (12)), but in the
1467 variance balance (Eq. (9)) in the divergence term TT_{var} respectively in Eq. (11a) and Eq.
1468 (11b). Even if terms $A_{h,var}$, $A_{z,var}$, II and III in Eq. (11a, 11b) were neglected, the estimation
1469 of the magnitude of the two remaining terms shows that neither the contribution of GP_{var} nor
1470 TT_{var} to the magnitude of $\overline{c_i'^2}$ is small (Table 2). Also, this analysis shows that a simple
1471 relation between I_s and one dominant term in a balance equation or by a certain process
1472 controlling the mixing of reactants does not exist. At least two or more processes can be
1473 identified, which always influence I_s in an indirect way, so that $I_s \cong -0.5$ is not reached in the
1474 field for such conditions. Therefore $|I_s|$ remains to be bounded below such values. In the
1475 following we show that such bounds of I_s are also in agreement with existing results from the
1476 field and from models, if they are presented as a function of the Damköhler number, e.g., of
1477 relations between time scales for transport/mixing and chemical reactions.

1478

1479

1480

1481 4.3 The Damköhler Dependence of the Intensity of Segregation

1482

1483 The relation between a transport/mixing time scale τ_t and the chemical reaction time scale,

1484 $\tau_c = (k_{ij} \cdot \overline{OH})^{-1}$, the Damköhler number

1485

$$Da_c = \tau_t / \tau_c$$

1486 is commonly chosen to classify I_s (e.g., Damköhler, 1957; Astarita, 1967; Komori et al., 1991;
1487 Verver et al., 2000; Vinuesa and Vilá – Guerau de Arellano, 2005). For reaction Eq. (4) the
1488 chemical time scale τ_c is well described by the knowledge of

1489

$$k_{ij} \approx \frac{170}{T} e^{409/T} \text{ [ppb}^{-1}\text{s}^{-1}\text{]}$$

1490 with a mean value of about $k_{ij} = 2.3 \text{ ppb}^{-1}\text{s}^{-1}$ in the temperature ranges for 25 July, 2003
1491 (DOY 206) of the ECHO 2003 (Dlugi et al., 2010, 2014) and 22 November of ATTO 2015
1492 studies. The magnitude of τ_t is often estimated by surface layer or ABL scalings (e.g., Stull,
1493 1988; Sorbjan, 1989; Raupach, 1988). For experiments above canopies near $z = h_c$, often a
1494 time scale



1495

$$\tau_{t_1} \approx h_c / u_* \quad (u_* = \text{friction velocity})$$

1496

is chosen (e.g., Patton et al., 2001). For this τ_t -scaling, Dlugi et al. (2014) determined Da_c in

1497

the range $0.01 < Da_c < 0.1$ for ECHO 2003. A revised analysis of the mixing conditions

1498

inside and directly above the mixed deciduous forest was performed based on diffusion

1499

experiments with tracer emissions at $z/h_c \approx 0.5$ and $z/h_c \approx 0.8$ during ECHO 2003. The

1500

results are compared to the wind tunnel experiments by Aubrun et al. (2005) and show that

1501

the diffusion time scale, τ_{t_2} (see also Koeltzsch, 1999), for mixing emissions from the leaves

1502

at heights $0.5 \leq z/h_c \leq 1$ to the measuring height at $z/h_c = 1.23$ is about three to four times

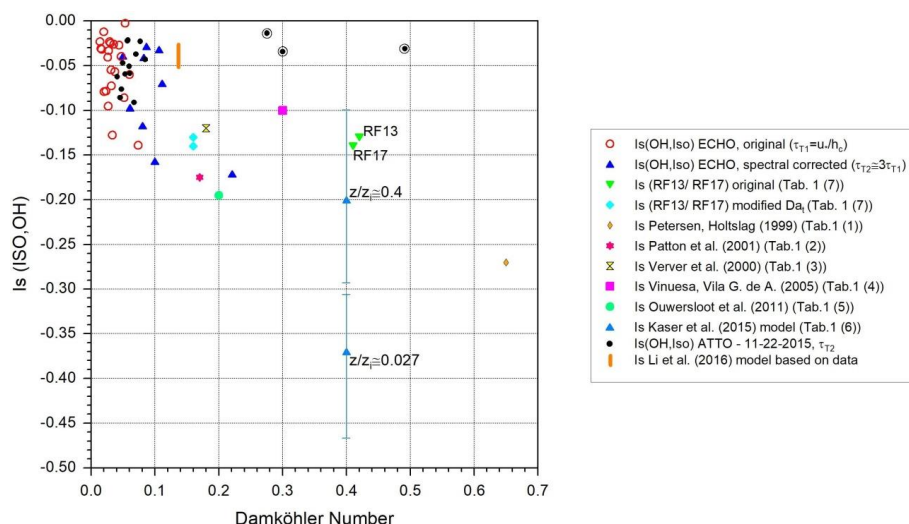
1503

larger than τ_{t_1} , e.g., $\tau_{t_2} \approx 3\tau_{t_1}$ (to $4\tau_{t_1}$). For illustration both time scales are given for ECHO

1504

2003 in Fig. 13, where experimental and model results are compared (Table 3).

1505



1506

1507

Fig. 13 The segregation intensity for reaction Eq. (4) as function of the Damköhler number Da_c for results given in Table 3 (numbers in brackets). (Three points from ATTO (circles) show smaller I_s than expected if the other data are considered. They represent low wind conditions where u_* scaling is a questionable choice and need additional analysis)

1510

1511

1512

1513

Kaser et al. (2015) give Da_c with

1514

$$\tau_t = z_i / w_*$$

1515

the ABL height z_i divided by the convective velocity scale, w_* (e.g., Stull, 1988; Garrett,

1516

1992) for RF13 and RF17. The measurements were performed at heights near $z/z_i \approx 0.4$,

1517

and not throughout the complete ABL. Therefore, for upward-directed motion a modified

1518

estimate with $\tau_t = 0.4(z_i/w_*)$ is applied in Fig. 13 to present their data. Li et al. (2016)

1519

calculated τ_t as originally done by Kaser et al. (2015). They present I_s - maxima for

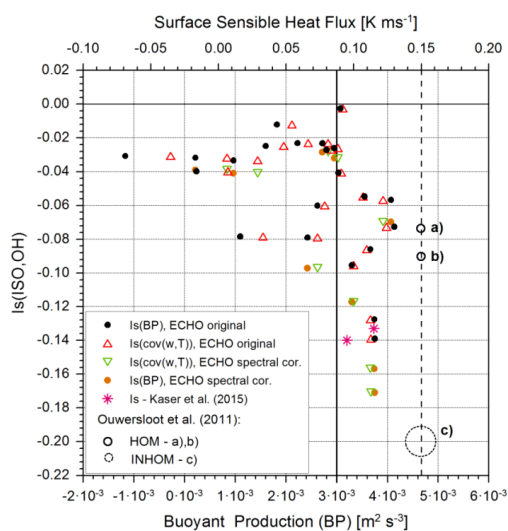


1520 $z/z_i \approx 300 \text{ m}/2100 \text{ m} \approx 0.14$. Therefore, with $\tau_t \approx 0.14(z_i/w_*)$ their results agree to the
 1521 range of other data in Fig. 13.

1522

1523 The model data (Table 3; Fig. 13) of Kaser et al. (2015) are given with their complete range
 1524 for $z/z_i \approx 0.4$ and the canopy top values for $z/z_i \approx 0.027$. Their near-surface values of I_s are
 1525 significantly larger than any other data for canopy top flow or surface layer conditions in the
 1526 literature (e.g., Ouwersloot et al., 2011; Vinuesa and Vilà-Guerau de Arellano, 2005; Patton
 1527 et al., 2001, Kim et al., 2016). Without the model data for $z/z_i \approx 0.027$, all other results agree
 1528 with a non-linear increase of I_s with increasing Da_c and the existence of a limiting range of
 1529 about $I_s < -0.35$ for $0.5 \leq Da_c \leq 2$ (Fig. 13). This empirical result agrees also with the
 1530 numerical fit according to a power function as shown in Fig. 12.

1531



1532

1533 **Fig. 14** The intensity of segregation as a function of buoyant production (BP) and the sensible heat
 1534 flux H . The dotted circle (c) and the data points labeled a) and b) indicate the range of
 1535 results presented by Ouwersloot et al. (2011) for homogeneous (HOM) and inhomogeneous
 1536 (INHOM) source distribution on the land surface. Also the average values reported by Kaser
 1537 et al. (2015) agree with this approach if the results from our CBL scaling analysis for H
 1538 are applied. $H > 0.078 \text{ K m s}^{-1}$ and $BP > 3 \cdot 10^{-3} \text{ m}^2 \text{ s}^{-3}$ describe the onset of convective
 1539 conditions at canopy top.

1540

1541

1542 In addition, $I_s(ISO, OH)$ can be empirically related to the buoyant production, BP , and also to
 1543 the turbulent sensible heat flux, H_s , near the surface (Dlugi et al., 2014). The agreement with
 1544 model results provided by Ouwersloot et al. (2011) becomes better (Fig. 14), if lower
 1545 frequency contributions are added as mentioned above (Fig. 12, 13). This spectral correction
 1546 with respect to the original ECHO results covers also the spectral range of I_s given by Kaser



1547 et al. (2015), if the results from our CBL-scaling analysis for the sensible heat flux are applied
1548 to their average I_s values (Fig. 14). Note that the data from ECHO 2003 in the range of
1549 $BP > 3 \cdot 10^{-3} m^2 s^{-3}$ represent NO_x mixing ratios below 2 ppb. The NOMADSS flights were
1550 performed in air masses with mean NO_x mixing ratios below about 0.6 ppb.

1551

1552

1553

1554 5. Summary and Conclusion

1555

1556 The published results from field studies on segregation and the new measurements from the
1557 ATTO site for the reaction of isoprene with OH are discussed and compared to models.
1558 Some statements made by Kaser et al. (2015) for their study in the ABL are compared to the
1559 available relationships obtained from the data analysis of field studies near canopy top and in
1560 the ABL to give a comprehensive overview and to identify possible natural limits on I_s based
1561 on theoretical considerations and the data available so far.

1562

1563 The intensity of segregation, I_s , appears to be (weakly) proportional to the isoprene flux only
1564 near canopy top, in agreement with an analysis for other scalar quantities described in the
1565 literature (see: Sections 3.3 and 4.1). For larger heights above the surface, this correlation
1566 becomes small, as not only the production term GP_{var} but also other terms contribute to the
1567 budget of isoprene variance as discussed in Section 3.3 and Section 4.1. An increase of I_s
1568 with increasing standard deviation of isoprene $\sigma_i = \overline{(c_i')^2}^{1/2}$ is observed near canopy top and
1569 also reported from modelling (e.g., Patton et al., 2001; Ouwersloot et al., 2011), but this
1570 increase is not exclusively related to an increasing isoprene flux.

1571

1572 In addition, the covariance $\overline{c_i'c_j'} = \overline{ISO'OH'}$ is non-linearly related to the product of the mean
1573 mixing ratios, $\overline{c_i} \times \overline{c_j} = \overline{ISO} \times \overline{OH}$. The data show an empirical relation of a power-law type
1574 (Fig. 12). This relation points towards an upper bound for I_s of about $|I_s| < 0.35$ near canopy
1575 top as well as in the ABL, a value which is most likely also related to the behavior of the
1576 correlation coefficient r_{ij} with increasing mixing ratios and I_s (Fig. 9). Therefore, the relation
1577 between experimentally determined $r_{ij,exp}$ and correlation coefficients applied or determined
1578 in model studies, $r_{ij,mod}$, $|r_{ij,exp}| < |r_{ij,mod}|$ needs further analysis. A comparable empirical
1579 upper limit for $I_s = f(Da_c)$ is obtained if experimental and model results of I_s are analyzed as
1580 function of the Damköhler number, Da_c . The empirical upper limit $|I_s| < 0.35$ is approached
1581 for $0.5 \leq Da_c \leq 2$. An extended analysis of the ECHO 2003 data proves that I_s has significant



1582 contributions in the frequency range between $4.5 \cdot 10^{-4} \text{ Hz}$ to $1.0 \cdot 10^{-3} \text{ Hz}$. Therefore
1583 absolute values of I_s increase by at least 15% compared to the results described by Dlugi et
1584 al (2014) for the range $1.7 \cdot 10^{-3} \text{ Hz} \leq r \leq 0.2 \text{ Hz}$. This trend is qualitatively visible in Fig. 13,
1585 with a tendency for surface measurements with smaller $|I_s|$ than given by modelling results
1586 that integrate over the ABL. Aircraft measurements that are also influenced by landscape
1587 heterogeneity exhibit relatively large values for I_s .

1588

1589 For the calculation of Da_c the concepts applied to determine the transport/mixing time scale
1590 need further analysis, as a simple formula like $\tau_{t_1} = h_c/u_*$ (or $\tau_{t_1} = z_i/w_*$) underestimates
1591 the time scales obtained from an analysis of diffusion experiments, at least for ECHO 2003
1592 and qualitatively also for the ATTO site.

1593

1594 It can be shown that for both case studies, ECHO 2003 and ATTO 2015, the contribution of
1595 ejections to the turbulent isoprene flux correlates with the two dominant terms $nvar(ISO)_{is}$
1596 and RE_{is} in the diagnostic equation for I_s . If in general only ejections contribute to I_s for a
1597 compound emitted by an inhomogeneous source, the magnitude of $|I_s|$ will be proportional to
1598 the percentage amount of ejections.

1599

1600 The observed increase of I_s with increasing buoyant production, BP , respectively with
1601 increasing surface sensible heat flux (Fig. 14) (Dlugi et al., 2014), is further improved if the
1602 extended spectral analysis for ECHO 2003 is compared to results from Kaser et al. (2015)
1603 and model data from Ouwersloot et al. (2011). Here, the surface sensible heat fluxes, H_s ,
1604 were calculated from Fig. S6 in Kaser et al. (2015) by CBL scaling for fluxes, as discussed in
1605 Section 3. Both results for the isoprene flux as well as the sensible heat flux are also
1606 comparable to measured fluxes in the same region as described by Su et al. (2015).
1607 Although there is no simple direct relation between I_s and BP - as given by a balance
1608 equation - higher values of I_s seem to appear generally at higher BP and H_s for convective
1609 conditions.

1610

1611 In summary, there are still only few measurements of segregation intensity (two ground
1612 based and one aircraft campaign), but in line with modelling studies some general
1613 tendencies could be established. Surface measurements show mostly I_s less than 18 % for
1614 10-min values. In line with the modelling studies and the aircraft measurements, by including
1615 longer time scales (lower frequencies) or larger spatial scales, I_s reaches larger values
1616 between 10 and 20 % (some extremes up to 30 %), also in line with a spectral representation
1617 of I_s given by Kaser et al. (2015). Therefore, one could argue that I_s is scale dependent for
1618 comparable turbulent conditions with, as a hypothesis,



$$|I_{s_homogeneous\ surface}| \leq |I_{s_inhomogeneous\ surface}|.$$

1620

1621 Some of the above findings may be particular to the considered reaction, as *OH* mixing ratios
1622 are always low compared to isoprene and both compounds exhibit a similar diurnal cycle
1623 driven by radiation (*OH*) and surface temperature (isoprene) which also serves to generate
1624 convection and turbulence, This might be one reason for the limits for I_s observed for this
1625 reaction in the boundary layer.

1626

1627

1628 Author contribution:

1629 RD, MB, MZ, HH, MA and MS initiated the study and developed the scientific concept of the
1630 study. RD, MB, CM, AT, MZ, OA, EB, AH, JK, GK, DM, MM, AN, EP, FR, ST, JW, AY-S, HH
1631 and MS performed the measurements and/or contributed to the data analysis with major
1632 contributions to study design, measurement setup, measurements and data analysis from
1633 ATTO and ECHO. HO contributed modeling results. All authors contributed to the discussion
1634 and interpretation of the results and to the writing of the paper.

1635

1636

1637 Competing interests:

1638 The authors declare that they have no conflict of interest.

1639

1640 Data availability: Data used in this publication can be accessed by contacting the
1641 corresponding authors. General information on the ATTO project as well as a link to the
1642 ATTO-data portal can be found at <https://www.attoproject.org/>.

1643

1644

1645

1646

1647

1648

Acknowledgement:

1649 We thank the Max Planck Society and the Instituto Nacional de Pesquisas da Amazonia for
1650 continuous support. We acknowledge the support by the German Federal Ministry of
1651 Education and Research (BMBF contract 01LB1001A) and the Brazilian Ministério de Ciência
1652 Tecnologia e inovação (MCTI/FINEP contract 01.11.01248.00) as well as the Amazon State
1653 University (UEA), FAPEAN, LBA/INPA and SDS/CEUC/RDS-Uatumã.

1654

1655 Ralph Dlugi, Martina Berger and Michael Zelger greatly acknowledge the financial
1656 support by the Max Planck Institute for Chemistry.

1657

1658 Nelson Luís Dias contributed by a very valuable discussion on concepts and methods of data
1659 analysis. We thank Thomas Klüpfel, Markus Rudolf, Michael Welling, Dieter Scharffe, Reiner
1660 Ditz, Stefan Wolff, Stephan Keßel, Thómas Chor and Lucas Emilio B. Hoeltgebaum for
1661 various supports preparing and performing the field study at the ATTO site, for data pre-
1662 processing and pre- analysis and Nicole Mölders and Eiko Nemitz for intensive discussion on
1663 various aspects of these topics.

1664
1665
1666
1667
1668

References

- 1669 André, J. C., De Moor, G., Lacarrère, P., and du Vachat, R.: Modeling the 24-Hour Evolution of the
1670 Mean and Turbulent Structures of the Planetary Boundary Layer, *J. Atmos. Sci.*, 35, 1861 –
1671 1883, [https://doi.org/10.1175/1520-0469\(1978\)035<1861:MTHEOT>2.0.CO;2](https://doi.org/10.1175/1520-0469(1978)035<1861:MTHEOT>2.0.CO;2), 1978
1672
- 1673 Andreae, M. O. Acevedo, O. C., Araújo, A., Artaxo, P., Barbosa, C. G. G., Barbosa, H. M. J., Brito, J.,
1674 Carbone, S., Chi, X., Cintra, B. B. L., da Silva, N. F., Dias, N. L., Dias-Júnior, C. Q., Ditas, F.,
1675 Ditz, R., Godoi, A. F. L., Godoi, R. H. M., Heimann, M., Hoffmann, T., Kesselmeier, J.,
1676 Könemann, T., Krüger, M. L., Lavric, J. V., Manzi, A. O., Moran-Zuloaga, D., Nölscher, A. C.,
1677 Santos Nogueira, D., Piedade, M. T. F., Pöhlker, C., Pöschl, U., Rizzo, L. V., Ro, C.-U.,
1678 Ruckteschler, N., Sá, L. D. A., Sá, M. D. O., Sales, C. B., Santos, R. M. N. D., Saturno, J.,
1679 Schöngart, J., Sörgel, M., de Souza, C. M., de Souza, R. A. F., Su, H., Targhetta, N., Tóta, J.,
1680 Trebs, I., Trumbore, S., van Eijck, A., Walter, D., Wang, Z., Weber, B., Williams, J.,
1681 Winderlich, J., Wittmann, F., Wolff, S., and Yáñez-Serrano, A. M.: The Amazon Tall Tower
1682 Observatory (ATTO) in the remote Amazon Basin: overview of first results from ecosystem
1683 ecology, meteorology, trace gas, and aerosol measurements, *Atmos. Chem. Phys. Discuss.*,
1684 15, 11599–11726, <https://doi.org/10.5194/acpd-15-11599-2015>, 2015
1685
- 1686 Antonia, R.A.: Conditional sampling in turbulence measurement. *Ann. Rev. Fluid Mech.* 13:131-156,
1687 <https://doi.org/10.1146/annurev.fl.13.010181.001023>, 1981
1688
- 1689 Ammann, C., Spirig, C., Neffel, A., Steinbacher, M., Komenda, M., and Schaub, A.: Application of
1690 PTR-MS for measurements of biogenic VOC in a deciduous forest, *Int. J. Mass Spectrom.*,
1691 239, 87–101, 2004
1692
- 1693 Astarita, G.: Mass transfer with chemical reaction, Elsevier, Amsterdam, 1967
1694
- 1695 Aubrun, S., Koppmann, R., Leitl, B., Möllmann-Coers, M., and Schaub, A.: Physical modelling of a
1696 complex forest area in a wind tunnel – comparison with field data, *Agr. Forest. Meteorol.*, 129,
1697 121–135, 2005
1698
- 1699 Beier, N., and Weber, M.: Turbulente Austauschprozesse in der Grenzschicht. Technical Report,
1700 Meteorologisches Institut, Universität München, Germany, 1992
1701
- 1702 Bencula, K., and Seinfeld, J.: On frequency distributions of air pollutant concentrations, *Atmos.*
1703 *Environ.*, 10, 941–950, 1976
1704
- 1705 Brune, W. H., Stevens, P. S., and Mather, J. H.: Measuring OH and HO₂ in the Troposphere by Laser-
1706 Induced Fluorescence at Low-Pressure, *J Atmos Sci*, 52, 3328-3336, [https://doi](https://doi.org/10.1175/1520-0469(1995)052<3328:Moahit>2.0.Co;2)
1707 [10.1175/1520-0469\(1995\)052<3328:Moahit>2.0.Co;2](https://doi.org/10.1175/1520-0469(1995)052<3328:Moahit>2.0.Co;2), 1995
1708
- 1709 Businger, J. A.: Turbulent transfer in the atmospheric surface layer. In: D. A. Hangen (Ed.): Workshop
1710 on Micrometeorology, Chapter 2, AMS, Bosten, USA, 1973
1711
- 1712 Butler, T. M., Taraborrelli, D., Brühl, C., Fischer, H., Harder, H., Martinez, M., Williams, J., Lawrence,
1713 M. G., and Lelieveld, J.: Improved simulation of isoprene oxidation chemistry with the
1714 ECHAM5/MESSy chemistry-climate model: lessons from the GABRIEL airborne field
1715 campaign, *Atmos. Chem. Phys.*, 8, 4529–4546, [https://doi:10.5194/acp-8-4529-2008](https://doi.org/10.5194/acp-8-4529-2008), 2008
1716
- 1717 Caughey, S. J., and Palmer, S. G.: Some aspects of turbulence structure through the depth of the
1718 convective boundary layer, *Quart J. Roy. Meteor. Soc.*, 105, 811-827,
1719 [https://doi:10.1002/qj.49710544606](https://doi.org/10.1002/qj.49710544606), 1979
1720



- 1721 Cava, D., Katul, G. G., Scrimieri, A., Poggi, D., Cescatti, A., and Giostra, U.: Buoyancy and the
1722 sensible heat flux budget within dense canopies, *Boundary Layer Meteorol.*, 118, 217 – 240,
1723 [https://doi: 10.1007/s10546-005-4736-1](https://doi.org/10.1007/s10546-005-4736-1), 2006
1724
- 1725 Ciccio, P., Fabozzi, C., Brancaleoni, E., Cecinato, A., Frattoni, M., Loreto, F., Kesselmeier, J.,
1726 Schäfer, L., Bode, K., Torres, L., and Fugit, J.-L.: Use of the isoprene algorithm for predicting
1727 the monoterpene emission from the Mediterranean holm oak *Quercus ilex* L.: Performance
1728 and limits of this approach, *J. Geophys. Res.*, 102, 23319–23328, 1997
1729
- 1730 Crosley, D. R.: The Measurement of Oh and Ho₂ in the Atmosphere, *J Atmos Sci*, 52, 3299-3314,
1731 [https://doi 10.1175/1520-0469\(1995\)052<3299:Tmooh>2.0.Co;2](https://doi.org/10.1175/1520-0469(1995)052<3299:Tmooh>2.0.Co;2), 1995
1732
- 1733 Cuijpers, J. W. M. and Holtslag, A. A. M.: Impact of Skewness and Nonlocal Effects on Scalar and
1734 Buoyancy Fluxes in Convective Boundary Layers. *J. Atmos. Sci.*, 55: 151-162, 1998
1735
- 1736 Damköhler, G.: Einfluß von Diffusion, Strömung und Wärmetransport auf die Ausbeute bei chemisch-
1737 technischen Reaktionen, VDI, Leverkusen, Germany, 126 pp., 1957
1738
- 1739 Danckwerts, P.: The definition and measurement of some characteristics of mixtures, *Appl. Sci. Res.*,
1740 3, 279–296, 1952
1741
- 1742 Deardorff, J. W.: Three-dimensional numerical study of turbulence in an entraining mixed layer,
1743 *Boundary Layer Meteorol.*, 7, 199 – 223, <https://doi.org/10.1007/BF00227913>, 1974
1744
- 1745 Dlugi, R., Berger, M., Zelger, M., Hofzumahaus, A., Siese, M., Holland, F., Wisthaler, A., Grabmer, W.,
1746 Hansel, A., Koppmann, R., Kramm, G., Möllmann-Coers, M., and Knaps, A.: Turbulent
1747 exchange and segregation of HO_x radicals and volatile organic compounds above a
1748 deciduous forest, *Atmos. Chem. Phys.*, 10, 6215–6235, [https://doi:10.5194/acp-10-6215-2010](https://doi.org/10.5194/acp-10-6215-2010),
1749 2010
1750
- 1751 Dlugi, R., Berger, M., Zelger, M., Hofzumahaus, A., Rohrer, F., Holland, F., Lu, K., and Kramm, G.:
1752 The balances of mixing ratios and segregation intensity: a case study from the field (ECHO
1753 2003), *Atmos. Chem. Phys.*, 14, [https://doi:10.5194/acp-14-10333-2014](https://doi.org/10.5194/acp-14-10333-2014), 2014
1754
- 1755 Donaldson, C. D.: On the modelling of the scalar correlation necessary to construct a second order
1756 closure description of turbulent reacting flows, in: *A review in turbulent mixing in non reactive
1757 and reactive flows*, edited by: Murthy, S., Plenum Press, New York, 1975
1758
- 1759 Donaldson, C. D., and Hilst, G.: Effect of inhomogeneous mixing on atmospheric photochemical
1760 reactions, *Environ. Sci. Technol.*, 6, 812–816, 1972
1761
- 1762 Doughty, C. E., and M. L. Goulden: Are tropical forests near a high temperature threshold?, *J.
1763 Geophys. Res.*, 113, G00B07, [https://doi:10.1029/2007JG000632](https://doi.org/10.1029/2007JG000632), 2008
1764
- 1765 Ebel, A., Memmesheimer, M., and Jakobs, H. J.: Chemical perturbations in the planetary boundary
1766 layer and their relevance for chemistry transport modelling, *Bound.-Lay. Meteorol.*, 125, 256–
1767 278, 2007
1768
- 1769 Eerdekens, G., Ganzeveld, L., Vilà-Guerau de Arellano, J., Klüpfel, T., Sinha, V., Yassaa, N., Williams,
1770 J., Harder, H., Kubistin, D., Martinez, M., and Lelieveld, J.: Flux estimates of isoprene,
1771 methanol and acetone from airborne PTR-MS measurements over the tropical rainforest
1772 during the GABRIEL 2005 campaign, *Atmos. Chem. Phys.*, 9, 4207-4227,
1773 <https://doi.org/10.5194/acp-9-4207-2009>, 2009
1774
- 1775 Finlayson-Pitts, B. J. and Pitts Jr., J. N.: *Atmospheric Chemistry: Fundamentals and Experimental
1776 Techniques*, J. Wiley & Sons, New York, 1986
1777
- 1778 Garratt, J. R.: *The Atmospheric Boundary Layer*, Cambridge University Press, UK, 1992
1779
- 1780 Gerken, T., Chamecki, M., and Fuentes, J. D.: Estudo da interação entre o transporte de compostos
1781 orgânicos voláteis biogênicos e química dentro de um dossel da floresta tropical utilizando



- 1782 Large Eddy Simulation, *Ciência e Natura*, Santa Maria v.38 Ed. Especial- IX Workshop
1783 Brasileiro de Micrometeorologia, p. 262 – 265, [https://doi: 10.5902/2179460X21577](https://doi.org/10.5902/2179460X21577), 2016
1784
- 1785 Guenther, A. , Hewitt, C. N., Erickson, D., Fall, R., Geron, C., Graedel, T., Harley, P., Klinger, L.,
1786 Lerda, M., McKay, W. A., Pierce, T., Scholes, B., Steinbrecher, R., Tallamraju, R., Taylor, J.,
1787 and Zimmerman, P. : A global model of natural volatile organic compound emissions, *J.*
1788 *Geophys. Res.*, 100, 8873–8892, <https://doi.org/10.1029/94JD02950>, 1995
1789
- 1790 Guenther, A. B., Jiang, X., Heald, C. L., Sakulyanontvittaya, T., Duhl, T., Emmons, L. K., and Wang, X.
1791 : The Model of Emissions of Gases and Aerosols from Nature version 2.1 (MEGAN2.1): an
1792 extended and updated framework for modeling biogenic emissions: *Geoscientific Model*
1793 *Development*, 5, 1471-1492, <https://doi:10.5194/gmd-5-1471-2012>, 2012
1794
- 1795 Hard, T. M., O'Brien, R. J., Chan, C. Y., and Mehrabzadeh, A. A.: Tropospheric Free-Radical
1796 Determination by Fage, *Environ Sci Technol*, 18, 768-777, <https://doi:10.1021/es00128a009>,
1797 1984
1798
- 1799 Haugen, D. A., (Ed.): *Workshop on Micrometeorology*, Amer. Meteor. Soc., 45 Beacon St., Boston,
1800 MA 02108. 392pp., 1973
1801
- 1802 Hens, K., Novelli, A., Martinez, M., Auld, J., Axinte, R., Bohn, B., Fischer, H., Keronen, P., Kubistin, D.,
1803 Nölscher, A. C., Oswald, R., Paasonen, P., Petaja, T., Regelin, E., Sander, R., Sinha, V.,
1804 Sipilä, M., Taraborrelli, D., Ernest, C. T., Williams, J., Lelieveld, J., and Harder, H.:
1805 Observation and modelling of HO_x radicals in a boreal forest, *Atmospheric Chemistry and*
1806 *Physics*, 14, 8723-8747, <https://doi:10.5194/acp-14-8723-2014>, 2014
1807
- 1808 Hess, G.D.: Observations and scaling of the atmospheric boundary layer, *Aust. Met. Mag.*, 41: 79-99,
1809 1992
1810
- 1811 Heus, T., and Jonker, H. J. J.: Subsiding Shells around Shallow Cumulus Clouds, *J. of the Atmos.*
1812 *Sci.*, 65, 1003 – 1017, <https://doi:10.1175/2007JAS2322.1>, 2008
1813
- 1814 Higgins, C. W., Katul, G. G., Froidevaux, M., Simeonov, V., and Parlange, M.B.: Are atmospheric
1815 surface layer flows ergodic? *Journal, Geophysical Research Letters*, 40, 3342–3346,
1816 <https://doi: 10.1002/grl.50642>, 2013
1817
- 1818 Hornbrook, R. S. , Crawford, J. H., Edwards, G. D., Goyea, O., Mauldin III, R. L., Olson, J. S., and
1819 Cantrell, C. A.: Measurements of tropospheric HO₂ and RO₂ by oxygen dilution modulation
1820 and chemical ionization mass spectrometry, *Atmos. Meas. Tech.*, 4, 735-756,
1821 <https://doi.org/10.5194/amt-4-735-2011>, 2011
1822
- 1823 Jiménez-Muñoz, J. C., Mattar, C., Barichivich, J., Santamaría-Artigas, A., Takahashi, K., Malhi, Y.,
1824 Sobrino, J. A., and van der Schrier, G.: Record-breaking warming and extreme drought in the
1825 Amazon rainforest during the course of El Niño 2015-2016, *Scientific reports* 6, 33130,
1826 <https://doi:10.1038/srep33130>, 2016
1827
- 1828 Kaimal, J. C., and Finnigan, J. J.: *Atmospheric Boundary Layer Flows: Their Structure and*
1829 *Measurement*, Oxford University Press, New York/Oxford, 289 pp., 1994
1830
- 1831 Karl, T. G. , Guenther, A., Yokelson, R. J., Greenberg, J., Potosnak, M., Blake, D. R., and Artaxo, P.:
1832 The tropical forest and fire emissions experiment: Emission, chemistry, and transport of
1833 biogenic volatile organic compounds in the lower atmosphere over Amazonia, *J. Geophys.*
1834 *Res.*, 112, D18302, <https://doi.org/10.1029/2007JD008539>, 2007
1835
- 1836 Karl, T., Misztal, P. K., Jonsson, H. H., Shertz, S., Goldstein, A. H., and Guenther, A. B.: Airborne flux
1837 measurements of BVOCs above Californian oak forests: Experimental investigation of surface
1838 and entrainment fluxes, OH densities, and Damköhler numbers, *J. Atmos. Sci.*, 70, 3277–
1839 3287, <https://doi:10.1175/JAS-D-13-054.1>, 2013
1840
- 1841 Kaser, L. , Karl, T., Yuan, B., Mauldin III, R. L., Cantrell, C. A., Guenther, A. B., Patton, E. G.,
1842 Weinheimer, A. J., Knote, C., Orlando, J., Emmons, L., Apel, E., Hornbrook, R., Shertz, S.,



- 1843 Ullmann, K., Hall, S., Graus, M., de Gouw, J., Zhou, X., and Ye, C.: Chemistry-turbulence
1844 interactions and mesoscale variability influence the cleansing efficiency of the atmosphere,
1845 Geophys. Res. Lett., 42 : 10,894 – 10,903, [https://doi: 10.1002/2015GL066641](https://doi.org/10.1002/2015GL066641), 2015
1846
- 1847 Katul, G.G., Hsieh, Ch. I., Kuhn, G., Ellsworth, D., and Nie, D.: Turbulent eddy motion at the forest-
1848 atmosphere interface. J Geophys Res 102: 13409-13421, 1997
1849
- 1850 Kesselmeier, J.: Exchange of Short-Chain Oxygenated Volatile Organic Compounds (VOCs) between
1851 Plants and the Atmosphere: A Compilation of Field and Laboratory Studies, J. Atmos. Chem.,
1852 39(3), 219 – 233, 2001
1853
- 1854 Kesselmeier, J., and Staudt, M.: Biogenic volatile organic compounds (VOC): An overview on
1855 emission, physiology and ecology, J. Atmos. Chem., 33, 23–88, 1999
1856
- 1857 Kim, S.-W., Barth, M. C., and Trainer, M.: Impact of turbulent mixing on isoprene chemistry, Geophys.
1858 Research Letters, 43, 7701 – 7708, [https://doi:10.1002/2016GL069752](https://doi.org/10.1002/2016GL069752), 2016
1859
- 1860 Koeltzsch, K.: On the relationship between the Lagrangian and Eulerian time scale, Atmos.
1861 Environment, 33: 117-128, 1998
1862
- 1863 Komori, S., Kanzaki, T., and Morakami, Y.: Simultaneous measurements on instantaneous
1864 concentrations of two reacting species in a turbulent flow with a rapid reaction, Phys. Fluids,
1865 A3, 507–510, 1991
1866
- 1867 Krol, M. C., Molemaker, M.-J., and Vilà Guerau de Arellano, J.: Effects of turbulence and
1868 heterogeneous emission on photochemically active species in the convective boundary layer,
1869 J. Geophys. Res., 105, 6871–6884, [https://doi:10.1029/1999JD900958](https://doi.org/10.1029/1999JD900958), 2000
1870
- 1871 Kramm, G.: Zum Austausch von Ozon und reaktiven Stickstoffverbindungen zwischen Atmosphäre
1872 und Biosphäre, Thesis, Humboldt University, Berlin, published as: Schriftenreihe des
1873 Fraunhofer-Instituts für Atmosphärische Umweltforschung, 34, ISBN: 3-927548-75-8, 1995
1874
- 1875 Kramm, G., and Meixner, F. X.: On the dispersion of trace species in the atmospheric boundary layer:
1876 A re-formulation of the governing equations for the turbulent flow of the compressible
1877 atmosphere, Tellus, 52A, 500–522, 2000
1878
- 1879 Lamb, R., and Seinfeld, J.: Modeling for urban air pollution – general theory, Environ. Sci. Technol., 7,
1880 253–261, 1973
1881
- 1882 Lamb, R., and Shu, W.: A Model of second order chemical reactions in turbulent fluid – part I:
1883 Formulation and Validation, Atmos. Environ., 12, 1685–1694, 1978
1884
- 1885 Lang, A. R. G., and Bradley, E. F.: Pressure covariance terms in the heat and moisture flux equations
1886 for local advection, Proc. 8th Australasian Fluid Mechanics Conference, Univ. of Newcastle,
1887 N.S.W., 28 November/ 2 December 1983, p. 1A.1 – 1A.4, 1983
1888
- 1889 Launder, B.E.: Heat and mass transport in Turbulence (ed. P. Bradshaw), 2nd edn., Springer Verlag,
1890 New York, 1978
1891
- 1892 Lenschow, D. H., Wyngaard, J. C., and Pennell, W. T.: Mean-Field and Second-Moment Budgets in a
1893 Baroclinic, Convective Boundary Layer, J. Atmos. Sci., 37, 1313–1326,
1894 [https://doi.org/10.1175/1520-0469\(1980\)037<1313:MFASMB>2.0.CO;2](https://doi.org/10.1175/1520-0469(1980)037<1313:MFASMB>2.0.CO;2), 1980
1895
- 1896 Lenschow, D. H.: Reactive trace species in the boundary layer from a micrometeorological
1897 perspective, J. Meteorol. Soc. Jpn., 60, 472–480, 1982
1898
- 1899 Li, Y., Barth, M. C., Chen, G., Patton, E. G., Kim, S.-W., Wisthaler, A., Mikoviny, T., Fried, A., Clark,
1900 R., Steiner, A. L.: Large-eddy simulation of biogenic VOC chemistry during the DISCOVER-
1901 AQ 2011 campaign, J. of Geophys. Research: Atmosphere, 121(13), 8083–8105,
1902 [https://doi:10.1002/2016JD024942](https://doi.org/10.1002/2016JD024942), 2016
1903



- 1904 Mallik, C., Tomsche, L., Bourtsoukidis, E., Crowley, J. N., Derstroff, B., Fischer, H., Hafermann, S.,
1905 Hueser, I., Javed, U., Kessel, S., Lelieveld, J., Martinez, M., Meusel, H., Novelli, A., Phillips, G.
1906 J., Pozzer, A., Reiffs, A., Sander, R., Taraborrelli, D., Sauvage, C., Schuladen, J., Su, H.,
1907 Williams, J., and Harder, H.: Oxidation processes in the Eastern Mediterranean atmosphere:
1908 Evidence from the Modelling of HO_x Measurements over Cyprus, Atmos. Chem. Phys., 2018,
1909 1-35, <https://doi.org/10.5194/acp-2018-25>, 2018.
- 1910
1911 Mao, J., Ren, X., Zhang, L., Van Duin, D. M., Cohen, R. C., Park, J. H., Goldstein, A. H., Paulot, F.,
1912 Beaver, M. R., Crouse, J. D., Wennberg, P. O., DiGangi, J. P., Henry, S. B., Keutsch, F. N.,
1913 Park, C., Schade, G. W., Wolfe, G. M., Thornton, J. A., and Brune, W. H.: Insights into
1914 hydroxyl measurements and atmospheric oxidation in a California forest, Atmospheric
1915 Chemistry and Physics, 12, 8009-8020, <https://doi.org/10.5194/acp-12-8009-2012>, 2012
- 1916
1917 Martinez, M., Harder, H., Kubistin, D., Rudolf, M., Bozem, H., Eerdeken, G., Fischer, H., Klupfel, T.,
1918 Gurk, C., Konigstedt, R., Parchatka, U., Schiller, C. L., Stickler, A., Williams, J., and Lelieveld,
1919 J.: Hydroxyl radicals in the tropical troposphere over the Suriname rainforest: airborne
1920 measurements, Atmospheric Chemistry and Physics, 10, 3759-3773, 2010
- 1921
1922 Mauldin III, R.L., Cantrell, C. A., Zondlo, M., Kosciuch, E., Eisele, F. L., Chen, G., Davis, D., Weber,
1923 R., Crawford, J., Blake, D., Bandy, A., and Thornton, D.: Highlights of OH, H₂SO₄, and
1924 methane sulfonic acid measurements made aboard the NASA P-3B during Transport and
1925 Chemical Evolution over the Pacific, J. Geophys. Res., 108(D20), 8796,
1926 <https://doi.org/10.1029/2003JD003410>, 2003
- 1927
1928 McBean, G. A., and Miyake, M.: Turbulent transfer mechanisms in the atmospheric surface layer,
1929 Quart. J. Meteorol. Soc., 98, 383 – 398, <https://doi.org/10.1002/qj.49709841610>, 1972
- 1930
1931 McRae, G., Goodin, W., and Seinfeld, J.: Mathematical modelling of photochemical air pollution, EQL-
1932 Report No.18, Tech. rep., California Inst.of Technology, Pasadena, 1982
- 1933
1934 Moeng, C.-H., and Sullivan, P. P.: A comparison of shear- and buoyancy-driven planetary boundary
1935 layer flows. J. Atmos. Sci., 51, 999–1022, 1994
- 1936
1937 Moeng, C.-H., and Wyngaard, J. C.: Statistics of conservative scalars in the convective boundary
1938 layer. J. Atmos. Sci., 41:3161 – 3169, 1984
- 1939
1940 Molemaker, M. J., and Vilà-Guerau de Arellano, J.: Control of chemical reactions by convective
1941 turbulence in the boundary layer. J. Atmos. Sci., 55, 568-579, 1998
- 1942
1943 Monin, A. S., and Obukhov, A. M.: Basic laws of turbulent mixing in the surface layer of the
1944 atmosphere. Trans. Geophys. Inst. Akad. Nauk. USSR, 151, 163–187, 1954
- 1945
1946 Monin, A. S., and Yaglom, A. M.: Statistical fluid mechanics, M.I.T. Press, Cambridge, Mass, 1971
- 1947
1948 Müller, J.-F., Stavrou, T., Wallens, S., De Smedt, I., Van Roozendaal, M., Potosnak, M. J., Rinne, J.,
1949 Munger, B., Goldstein, A., and Guenther, A. B.: Global isoprene emissions estimated using
1950 MEGAN, ECMWF analyses and a detailed canopy environment model, Atmos. Chem. Phys.,
1951 8, 1329–1341, <https://doi.org/10.5194/acp-8-1329-2008>, 2008
- 1952
1953 Nakagawa, H., and Nezu, I.: Prediction of the contributions to the Reynolds stress from bursting
1954 events in open-channel flows, J. Fluid Mech. 80, 99-128,
1955 <https://doi.org/10.1017/S0022112077001554>, 1977
- 1956
1957 Nölscher, A.C., Yañez-Serrano, A.M., Wolff, S., Carioca de Araujo, A., Lavrič, J.V., Kesselmeier, J.,
1958 and Williams, J.: Unexpected seasonality in quantity and composition of Amazon rainforest air
1959 reactivity, nature communication, 7:10383, <https://doi.org/10.1038/ncomms10383>, 2015
- 1960
1961 Novelli, A., Hens, K., Ernest, C. T., Kubistin, D., Regelin, E., Elste, T., Plass-Dulmer, C., Martinez, M.,
1962 Lelieveld, J., and Harder, H.: Characterisation of an inlet pre-injector laser-induced
1963 fluorescence instrument for the measurement of atmospheric hydroxyl radicals, Atmos Meas
1964 Tech, 7, 3413-3430, <https://doi.org/10.5194/amt-7-3413-2014>, 2014



- 1965
1966 O'Brien, E. E.: Turbulent mixing of two rapidly reacting chemical species, *Phys. Fluids*, 14, 1326–
1967 1331, 1971
1968
1969 Ouwersloot, H. G., Vilà-Guerau de Arellano, J., van Heerwaarden, C. C., Ganzeveld, L. N., Krol, M.
1970 C., and Lelieveld, J.: On the segregation of chemical species in a clear boundary layer over
1971 heterogeneous land surfaces, *Atmos. Chem. Phys.*, 11, 10681 – 10704,
1972 <https://doi.org/10.5194/acp-11-10681-2011>, 2011
1973
1974 Ouwersloot, H. G., Vilà-Guerau de Arellano, J., van Stratum, B. J. H., Krol, M. C., and Lelieveld, J.:
1975 Quantifying the transport of subcloud layer reactants by shallow cumulus clouds over the
1976 Amazon, *J. Geophys. Res.*, 118, 13.041–13.059, <https://doi.org/10.1002/2013JD020431>, 2013
1977
1978 Patton, E. G., Davis, K.J., Barth, M.C., and Sullivan, P.P.: Decaying scalars emitted by a forest canopy:
1979 A numerical study, *Bound-Lay. Meteorol.*, 100, 91–129, 2011
1980
1981 Patton, E. G., Sullivan, P. P., and Davis, K. J.: The influence of a forest canopy on top-down and
1982 bottom-up diffusion in the planetary boundary layer. *Q. J. R. Meteorol. Soc.*, 129: 1415 – 1434,
1983 <https://doi.org/10.1256/qj.01.175>, 2003
1984
1985 Panofsky, H. A. and Dutton, J. A.: *Atmospheric Turbulence*. J. Wiley, New York, 397 p., 1984
1986
1987 Poggi, D., Katul, G. G., and Albertson, J. D.: Momentum transfer and turbulent kinetic energy budgets
1988 within a dense model canopy, *Boundary-Layer Meteorology*, 111(3), 589-614
1989 <https://doi.org/10.1023/B:BOUN.0000016502.52590.af>, 2004
1990
1991 Pugh, T. A. M., MacKenzie, A. R., Langford, B., Nemitz, E., Misztal, P. K., and Hewitt, C. N.: The
1992 influence of small-scale variations in isoprene concentrations on atmospheric chemistry over a
1993 tropical rainforest, *Atmos. Chem. Phys.*, 11, 4121–4134, [https://doi.org/10.5194/acp-11-4121-](https://doi.org/10.5194/acp-11-4121-2011)
1994 [2011](https://doi.org/10.5194/acp-11-4121-2011), 2011
1995
1996 Ramos da Silva, R., Gandu, A. W., Sa, L. D. A., and Dias, M. A. F.: Cloud streets and land–water
1997 interactions in the Amazon, *Biogeochemistry*, 105, 201–211, [https://doi.org/10.1007/s10533-](https://doi.org/10.1007/s10533-011-9580-4)
1998 [011-9580-4](https://doi.org/10.1007/s10533-011-9580-4), 2011
1999
2000 Raupach, M. R.: Conditional statistics of Reynolds stress in rough-wall and smooth-wall turbulent
2001 boundary layers, *J. Fluid Mech.*, 108, 363 – 382, <https://doi.org/10.1017/S0022112081002164>,
2002 1981
2003
2004 Raupach, M. R.: Canopy transport processes, in: *Flow and Transport in the Natural Environment:*
2005 *Advances and Applications*, edited by: Steffen, W. L. and Denmead, O. T., Springer, Berlin,
2006 Germany, 95–127, 1988
2007
2008 Raupach, M. R., Antonia, R. A., and Rajagopalan, S.: Rough-wall turbulent boundary layers. *Appl.*
2009 *Mech. Rev.*, 44:1 – 25, 1991
2010
2011 Raupach, M. R., Finnigan, J. J., and Brunet, Y.: Coherent eddies and turbulence in vegetation
2012 canopies: The mixing layer analogy, *Bound.-Lay. Meteorol.*, 78, 351–382, 1996
2013
2014 Reynolds, O.: On the Dynamical Theory of Incompressible Viscous Fluids and the Determination of
2015 the Criterion, *Phil. Trans. Roy. Soc. London, A* 186, 123 – 164, (Roy. Soc.,
2016 <https://doi.org/10.1098/rsta.1895.0004>), 1895
2017
2018 Richardson, L. F.: The Supply of Energy from and to Atmospheric Eddies, *Proc. Roy. Soc., A*, 97, 354
2019 – 373 (Roy. Soc., <https://doi.org/10.1098/rspa.1920.0039>), 1920
2020
2021 Rohrer, F., Lu, K., Hofzumahaus, A., Bohn, B., Brauers, T., Chang, C.-C., Fuchs, H., Häseler, R.,
2022 Holland, F., Hu, M., Kita, K., Kondo, Y., Li, L., Lou, S., Oebel, A., Shao, M., Zeng, L., Zhu, T.,
2023 Zhang, Y., and Wahner, A.: Maximum efficiency in the hydroxyl-radical-based self-cleansing of
2024 the troposphere, *Nature Geoscience*, 7, 559–563, <https://doi.org/10.1038/ngeo2199>, 2014
2025



- 2026 Sachs, L., and Hedderich, J.: *Angewandte Statistik*, Springer, Berlin, Heidelberg, New York, 2006
2027
- 2028 Schaub, A.: *Untersuchung von Isopren und dessen Oxidationsprodukten in und oberhalb eines*
2029 *Mischwaldes*, Ph.D. thesis, Mathematisch-Naturwissenschaftliche Fakultät, Universität Köln,
2030 Germany, 2007
2031
- 2032 Schumann, U.: Large-eddy simulation of turbulent diffusion with chemical reactions in the convective
2033 boundary layer, *Atmos. Environ.*, 23, 1713–1729, 1989
2034
- 2035 Seinfeld, J. H. and Pandis, S. N.: *Atmospheric Chemistry and Physics*, John Wiley & Sons, New
2036 York/Chichester/Weilheim/Brisbane/Singapore/Toronto, 1997
2037
- 2038 Shaw, R.H. , Paw, K. T. U., Zhang, X. J., Gao, W., Den Hartog, G., Neumann, H. H.: Retrieval of
2039 turbulent pressure fluctuations at the ground surface beneath a forest, *Boundary Layer*
2040 *Meteorol.*, 50, 319 – 338, <https://doi.org/10.1007/BF00120528>, 1990
2041
- 2042 Shu, W.: *Turbulent chemical reactions: Application to atmospheric chemistry*, Ph.D. thesis, Dept.
2043 Chem. Eng., Caltec, Pasadena, 1976
2044
- 2045 Sindelarova, K., Granier, C., Bouarar, I., Guenther, A., Tilmes, S., Stavrou, T., Muller, J. F., Kuhn,
2046 U., Stefani, P., and Knorr, W.: Global data set of biogenic VOC emissions calculated by the
2047 MEGAN model over the last 30 years, *Atmos. Chem. Phys.*, 14, 9317-9341,
2048 <https://doi.org/10.5194/acp-14-9317-2014>, 2014
2049
- 2050 Sorbjan, Z.: *Structure of the atmospheric boundary layer*, Prentice Hall, N. J., USA, 1989
2051
- 2052 Spirig, C., Neftel, A., Ammann, C., Dommen, J., Grabmer, W., Thielmann, A., Schaub, A.,
2053 Beauchamp, J., Wisthaler, A., and Hansel, A.: Eddy covariance flux measurements of biogenic
2054 VOCs during ECHO 2003 using proton transfer reaction mass spectrometry, *Atmos. Chem.*
2055 *Phys.*, 5, 465–481, <https://doi.org/10.5194/acp-5-465-2005>, 2005
2056
- 2057 Stull, R. B.: *An Introduction to Boundary Layer Meteorology (Atmospheric Sciences Library)*, Springer,
2058 1988
2059
- 2060 Su, L. , Patton, E. G., Vilà-Guerau de Arellano, J., Guenther, A. B., Kaser, L., Yuan, B., Xiong, F.,
2061 Shepson, P. B., Zhang, L., Miller, D. O., Brune, W. H., Baumann, K., Edgerton, E.,
2062 Weinheimer, A., and Mak, J. E.: Understanding isoprene photo-oxidation using observations
2063 and modelling over a subtropical forest in the Southeast US. *Atmos. Chem. Phys.*, 16, 7725-
2064 7741, <https://doi.org/10.5194/acp-16-7725-2016>, 2016
2065
- 2066 Sun, J.: Tilt correction over complex terrain and their implication for CO₂-transport, *Bound.-Lay.*
2067 *Meteorol.*, 124, 143–159, 2007
2068
- 2069 Sykes, R. I., Parker, S. F., Henna, D. S., and Lewellen, W. S.: Turbulent Mixing with Chemical
2070 Reaction in the Planetary Boundary Layer, *J. Appl. Meteorol.*, 33, 825–834, 1994
2071
- 2072 van Stratum, B. J. H., Vilà-Guerau de Arellano, J., Ouwersloot, H. G., van den Dries, K., van Laar, T.
2073 W., Martinez, M., Lelieveld, J., Diesch, J.-M., Drewnick, F., Fischer, H., Hosaynali Beygi, Z.,
2074 Harder, H., Regelin, E., Sinha, V., Adame, J. A., Sörgel, M., Sander, R., Bozem, H., Song, W.,
2075 Williams, J., and Yassaa, N.: Case study of the diurnal variability of chemically active species
2076 with respect to boundary layer dynamics during DOMINO, *Atmos. Chem. Phys.*, 12, 5329–
2077 5341, <https://doi.org/10.5194/acp-12-5329-2012>, 2012
2078
- 2079 Verver, G., van Dop, H., and Holtslag, A.: Turbulent mixing of reactive gases in the convective
2080 boundary layer, *Bound.-Lay. Meteorol.*, 85, 197–222, 1997
2081
- 2082 Verver, G. H. L., van Dop, H., and Holtslag, A. A. M.: Turbulent mixing and the chemical breakdown of
2083 isoprene in the atmospheric boundary layer, *J. Geophys. Res.*, 105, 3983–4002, 2000
2084



- 2085 Vilà-Guerau de Arellano, J., Duynkerke, P., and Builtjes, P.: The divergence of the turbulent diffusion
2086 flux in the surface layer due to chemical reactions: The NO-O₃-NO₂ system, *Tellus*, 43, 22–
2087 23, 1993
2088
- 2089 Vinuesa, J.-F. and J. Vila-Guerau de Arellano: Introducing effective reaction rates to account for the
2090 inefficient mixing of the convective boundary layer. *Atmos. Environ.*, 39: 445–461, 2005
2091
- 2092 Wahrhaft, Z.: Passive scalars in turbulent flows, *Annu. Rev. Fluid Mech.*, 32, 203–240, 2000
2093
- 2094 Wang, G., and Hendon, H. H.: Why 2015 was a strong El Niño and 2014 was not, *Geophys. Res. Lett.*
2095 93, 63, <https://doi.org/10.1002/2017GL074244>, 2017
2096
- 2097 Wu, Z., Huang, N. E., Long, S. R., and Peng, C.-K.: On the trend, detrending, and variability of
2098 nonlinear and nonstationary time series. *PNAS*, 104, 14889 – 14894, [https://doi.org](https://doi.org/10.1073/pnas.0701020104)
2099 [/10.1073/pnas.0701020104](https://doi.org/10.1073/pnas.0701020104), 2007
2100
- 2101 Wyngaard, J.C.: Boundary- Layer Modelling. Lecture Notes on Atmospheric Turbulence and Air
2102 Pollution Modelling, D. Riedel, Dordrecht, The Netherlands, Chap. 3, 1982
2103
- 2104 Wyngaard, J.C.: Structure of the atmospheric boundary layer and implications for its modeling.
2105 *J. Climate Applied Meteorology*, 24:1131 –1142, 1985
2106
- 2107 Wyngaard, J., and Brost, R. A.: Top-down and bottom-up diffusion of a scalar in the convective
2108 boundary layer. *J. Atmos. Sci.*, 41, 102-112, [https://doi.org/10.1175/1520-](https://doi.org/10.1175/1520-0469(1984)041<0102:TDABUD>2.0.CO;2)
2109 [0469\(1984\)041<0102:TDABUD>2.0.CO;2](https://doi.org/10.1175/1520-0469(1984)041<0102:TDABUD>2.0.CO;2), 1984
2110
- 2111 Yáñez-Serrano, A. M., Nölscher, A. C., Williams, J., Wolff, S., Alves, E., Martins, G. A., Bourtsoukidis,
2112 E., Brito, J., Jardine, K., Artaxo, P., and Kesselmeier, J.: Diel and seasonal changes of
2113 biogenic volatile organic compounds within and above an Amazonian rainforest, *Atmos.*
2114 *Chem. Phys.*, 15, 3359-3378, <https://doi.org/10.5194/acp-15-3359-2015>, 2015
2115
- 2116 Zhou, M. Y., Lenschow, D. H., Stankov, B. B., Kaimal, J. C. and Gaynor, J. E.: Wave and turbulence
2117 structure in a shallow baroclinic convective boundary layer and overlying inversion, *J. Atmos.*
2118 *Sci.*, 42, 47–57, [https://doi.org/10.1175/1520-0469\(1985\)042<3C0047:WATSIA>3E2.0.CO;2](https://doi.org/10.1175/1520-0469(1985)042<3C0047:WATSIA>3E2.0.CO;2),
2119 1985
2120
2121